ANALYZING BURIED REINFORCED CONCRETE STRUCTURES SUBJECTED TO GROUND SHOCK FROM UNDERGROUND LOCALIZED EXPLOSIONS

By

NICHOLAS HENRIQUEZ

A THESIS PRESENTED TO THE GRADUATE SCHOOL
OF THE UNIVERSITY OF FLORIDA IN PARTIAL FULFILLMENT
OF THE REQUIREMENTS FOR THE DEGREE OF
MASTER OF SCIENCE

UNIVERSITY OF FLORIDA

2009

To 1504

ACKNOWLEDGMENTS

I thank my chair and advisor Dr. Theodor Krauthammer for first introducing me to the study of protective structures, as well as for his guidance with this report. I would also like to thank Dr. Serdar Astarlioglu for all of his assistance with the creation of the program and suggestions for improvement.

The financial support for this study provided by the U.S. Army Engineer Research and Development Center is gratefully acknowledged.

I especially need to thank my family and friends for all of their support.

TABLE OF CONTENTS

page

LIST OF TABLES

LIST OF FIGURES

LIST OF SYMBOLS

A_c	Cross-sectional area of concrete
A_{sb}	Area of reinforcement
A_i	Area of a layer
C	Damping
c	Elastic wave velocity
c	Seismic velocity
c	Neutral axis depth at Section 1
c'	Neutral axis depth at Section 2
C_c	Concrete compressive force of section 1
C'_c	Concrete compressive force of section 2
C_s	Steel compressive force of section 1
C'_s	Steel compressive force of section 2
d	Depth to steel layer
d	Soil layer thickness
d_b	Bar diameter
E	Modulus of elasticity
E_c	Concrete modulus of elasticity
f	Coupling factor
f_i	Stress in a layer
f'_s	Tensile strength of reinforcement
f_y	Yield strength of reinforcement
$f'c$	Concrete cylinder strength
F_{cc}	Total compressive concrete force in a section
F_i	Force in a layer

F_{sc}	Total compressive steel force in a section
F_{st}	Total tensile steel force in a section
F_t	Total force
$F_e(t)$	Equivalent forcing function
h	Slab thickness
I	Moment of inertia
K_0	Coefficient of lateral earth pressure
K_L	Load factor
K_m	Mass factor
L	Length of shorter dimension of box wall
L	Length of structure
l	Strip length
L_x	Length of slab in the x-direction
L_y	Length of slab in the y-direction
m	Unit mass
M_e	Equivalent mass
M_t	Total mass
m_c	Moment in a concrete layer
m_s	Moment in a steel layer
m_u	Total internal moment about the neutral axis
N	Thrust force
n	Attenuation coefficient
n_u	Total membrane force
$P(t)$	Pressure function
$p(x)$	Pressure function

P_0	Peak free-field pressure
$P_{wall}\ (t)$	Pressure function on the wall
R	Range
$R(x)$	Dynamic resistance function
S	Surround stiffness
t	Lateral movement of strip
t_a	Load arrival time
T	Steel tensile force of section 1
T'	Steel tensile force of section 2
T_x	Yield force per unit-width in the x-direction
T_y	Yield force per unit-width in the y-direction
u_I	Incident normal particle displacement
u_R	Reflected normal particle displacement
u_T	Reflected normal particle displacement
$\dot{u}$	Normal particle velocity
$\dot{u}_I$	Incident normal particle velocity
$\dot{u}_R$	Reflected normal particle velocity
$\dot{u}_T$	Reflected normal particle velocity
V	Shear force
W	Equivalent charge weight
w	Beam displacement
w	Distributed load on the strip
x	Displacement
$\dot{x}$	Velocity

$\ddot{x}$	Acceleration
β	Newmark-Beta integration constant
β	Portion of slab length between central and support plastic hinges
β_1	Ratio of ACI stress block depth to neutral-axis depth
δ	Central deflection of strip
$\Delta_{\max}$	Maximum deflection at wall center
$\Delta_{\max}$	Maximum shear slip
Δz	Thickness of concrete layer
ε	Axial strain
ε_c	Concrete strain
ε_{cu}	Concrete strain at failure
ε_i	Strain in a layer
ε_s	Steel strain
θ	Direction angle of an elastic wave
θ	End rotation
ρ	Material density
ρ_0	Soil density
ρ_{vt}	Ratio of total reinforcement area to the area of the plane it crosses
σ	Normal stress
σ_I	Incident normal stress
σ_R	Reflected normal stress
σ_T	Transmitted normal stress
τ_e	Elastic direct shear resistance

τ_L	Limiting direct shear capacity
τ_m	Maximum direct shear resistance
ϕ	Friction angle of soil
$\phi(x)$	Shape function

Abstract of Thesis Presented to the Graduate School
of the University of Florida in Partial Fulfillment of the
Requirements for the Degree of Master of Science

ANALYZING BURIED REINFORCED CONCRETE STRUCTURES SUBJECTED TO GROUND SHOCK FROM UNDERGROUND LOCALIZED EXPLOSIONS

By

Nicholas Henriquez

August 2009

Chair: Theodor Krauthammer
Major: Civil Engineering

Close-in localized HE detonations pose a substantial risk to buried RC box-type structures. This study investigated the relationships between the HE charge and its distance from an RC box wall, the existing soil layers and their properties, the direct-induced ground shock transmitted through soil layers, the load distribution on the structural wall, and the structural behavior. Previous experimental studies were examined and their results were compared with those obtained from the computer code Dynamic Structural Analysis Suite (DSAS) that was modified to handle such complicated conditions. The box structure was represented in DSAS by addressing the wall slab as a single degree of freedom system, while the effects of adjacent structural components were incorporated into the resistance function for the wall. The spatial dynamic pressure distribution on the wall was processed to derive an equivalent uniformly-distributed dynamic pressure on the wall to be used for the fully nonlinear structural analyses.

CHAPTER 1
INTRODUCTION

1.1 Problem Statement

Having a military structure located underground achieves more than just concealment. Burying a structure allows the builders to make use of the ground's natural damping to absorb and dissipate the blast wave energy from a munitions explosion. Most commonly, these buried structures take the form of a box, built using reinforced concrete.

These types of concrete structures are common for defense against conventional and nuclear weapons. Should a buried box fail, it could result in the loss of human lives. Also, munitions and other supplies may be stored in these facilities, the loss of which might lead to a supply shortage.

Analytical methods and computer programs which are meant to examine the effects of buried explosions on buried-box structures exist, but they have drawbacks. More complex programs, such as finite element codes or hydrocodes, consider a high number of degrees of freedom and are computationally intensive. These programs may model the soil using finite elements, assuming a uniform soil type. Since the soil properties will be neither uniform nor able to be characterized by a simple material model, the results that these programs give for the transmission of the blast wave may or may not be more accurate than using empirical equations, and the amount of time and memory required to track all of the soil nodes can be excessive.

A method to analyze quickly but accurately the effects of a buried blast on a buried box would be ideal for use during a preliminary design phase, as it would save time. Use of a single-degree-of-freedom (SDOF) model would aid in achieving this goal, since calculations on such a model can be performed quickly.

1.2 Objective and Scope

The objective of this work is to develop an SDOF computational approach to analyze quickly and accurately the dynamic response of a buried reinforced concrete (RC) structure to a buried explosive's blast loads, using a rational resistance function and including different modes of response. Doing so will aid in the proper selection of materials and layout to protect the structure against common or predicted explosions. Such factors include concrete strength and concrete thickness in the structure's walls, steel reinforcement, and soil backfill for the structure's location. The loads on the structure, its deflection, and its flexural and direct shear modes will be analyzed over the course of the explosion event.

This study is limited to a localized buried explosion whose most severe loads would occur near the center of one of the box's sides. The effects of a blast on the corners or roof of a box are not considered. The load on the wall will be approximated as a uniformly distributed load. The side walls of the box structure will be treated as slabs with axial and lateral forces caused by the effects of the blast. The use of up to three layers of soil will be allowed, with the box located in either of the two upper layers or spanning across both. The proposed methods will be compared with available test data.

1.3 Research Significance

This work can provide a simple, accurate procedure to dynamically analyze a buried RC box structure subjected to an underground blast loading. The method creates a time history of both the loads on the wall and the response of the center point of the wall, using an SDOF computational model that considers both flexure and direct shear behaviors.

CHAPTER 2
BACKGROUND AND LITERATURE REVIEW

2.1 Introduction

Burying a structure provides a good measure of protection against airblast. If an explosive device is able to penetrate into the ground before detonation, however, it can exert a much greater load on the structure and present a significant danger. An adequate thickness of concrete and reinforcing steel must be provided to protect against these threats.

During the design phase of an RC box, the possible threats are usually known or assumed. These threats can then be simplified to a design load on the boxes. With this information, the chosen box design can be evaluated by analyzing the relevant structural response modes.

This study is focused on buried RC boxes whose outer side walls are loaded by a buried explosion. Section 2.2 of this review discusses the use of an SDOF system. In Sections 2.3 and 2.4, the two most likely structural response modes, flexure and direct shear, are discussed. A review of blast loading and the specifics of underground blasts are presented in Section 2.5. Reflection and transmission of elastic waves are discussed in Section 2.6.

2.2 Single Degree of Freedom (SDOF) Systems

For both simplicity and speed of calculations, it is advantageous to analyze a wall of the buried box structure as an SDOF system. This type of system is an approximation of reality, where a nearly infinite number of degrees of freedom exists. An SDOF system involves motion in only one direction, which, in this case, is the wall's movement. Figure 2-1 shows an idealized damped SDOF system.

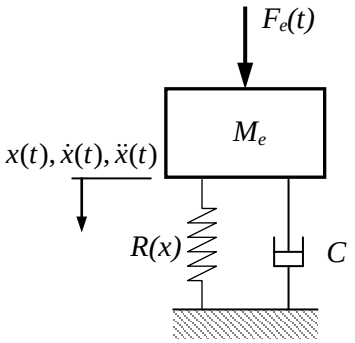

Figure 2-1. SDOF system

In an SDOF system, there is only one mass, resistance function, and damper, and this mass is acted upon by a single forcing function. Each of these is the SDOF equivalent of the total mass, force, etc. The degree of freedom is the vertical displacement, x. M_e is the equivalent mass, $F_e(t)$ the equivalent forcing function, C the damping, and $R(x)$ the resistance function. Often, it is possible to combine all the existing masses, springs, and dampers into this kind of simple case. By converting a more complicated system into an SDOF system, calculations are simplified. To be useful, the displacement term must correspond to the portion of the element that deflects the most, such as the midpoint on a simple beam, or the center portion of a wall or slab.

The motion of an SDOF system (with damping) is defined by the following forcing function:

$$F_e(t) = M_e \ddot{x} + C \dot{x} + R(x) \tag{2-1}$$

where the first derivative of the displacement term x is velocity and the second derivative is acceleration. In this case, the forcing function is created by the pressure wave in the ground. A conversion is required to calculate the SDOF equivalents of the real values of the total mass and forcing function. The total and equivalent masses of the system can be calculated using the following equations (Biggs 1964):

$$M_t = \int_L m(x)\,dx \tag{2-2}$$

$$M_e = \int_L m\phi^2(x)\,dx \tag{2-3}$$

where M_t is the total mass, M_e the equivalent mass, L the length, m the unit mass, and $\phi(x)$ the shape function.

The mass factor, K_M, is defined as the ratio of the equivalent mass to the total mass:

$$K_M = \frac{M_e}{M_t} \tag{2-4}$$

The total and equivalent loading functions and load factor can be found with the following equations:

$$F_t = \int_L p(x)\,dx \tag{2-5}$$

$$F_e = \int_L p(x)\phi(x)\,d \tag{2-6}$$

$$K_L = \frac{F_e}{F_t} \tag{2-7}$$

where F_t is the total load, F_e the equivalent load, K_L the load factor, and $p(x)$ the pressure function.

Tables of value of mass and load factors for structural elements with different support conditions at elastic, plastic, or elastoplastic states are found in Biggs (1964).

2.3 Flexure in Reinforced Concrete Walls

For the purpose of analysis, it is possible to treat the side walls of the buried box as laterally-restrained RC slabs. These slabs have two possible failure modes. The first, flexure, is discussed in this section. The second, direct shear, is discussed in the next section.

Figure 2-2 shows the resistance function of a laterally restrained RC slab. The yield line pattern, which is further discussed below, develops between points A and B. According to Johansen's yield line theory, the slab should have yielded when it first reached a load equal to the load at point C. However, the slab experiences an enhanced strength at B due to compressive membrane forces, caused by the lateral restraint. After peaking at point B, if load is still applied, there is a reduction in the compression membrane forces until point C. As point C is reached, cracks in the concrete extend all the way through the slab's depth. The compressive membrane forces in the concrete become tensile membrane forces. The tensile load near the slab's center is carried by the steel reinforcing, strengthened by the concrete pieces still bonded to it. The slab can then carry an increasing load while continuing to deflect, until failure occurs at point D. Depending on the amount of steel reinforcing, it is possible that this failure load may be even greater than the load at point B.

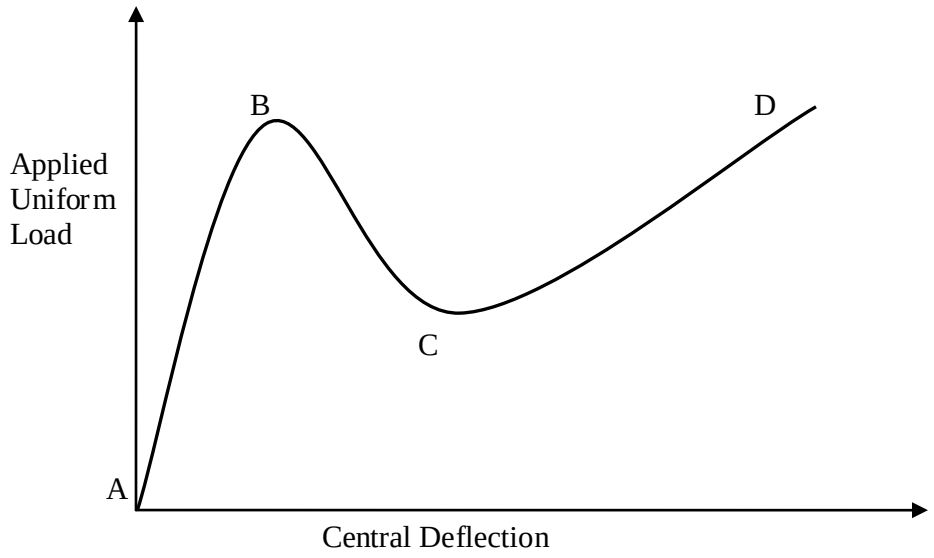

Figure 2-2. Load-deflection diagram for an RC slab

Due to the composition and support conditions of an RC slab, when a uniform load is applied, the slab wants to rotate about all of its supports. This results in a 45° yield pattern,

which can be seen in Figure 2-3. For analysis, the slab can be divided into individually-evaluated unit-width strips in both the x- and y-directions.

Each of the strips shown in Figure 2-3 can be analyzed as a beam with proper boundary conditions, using the plastic deformation explained in Park and Gamble (2000). The boundary conditions restrain rotation and vertical translation; however, minimal horizontal translation is allowed. In order for there to be a rotation at the end of the beams, plastic hinges must be formed. This is illustrated in Figure 2-4.

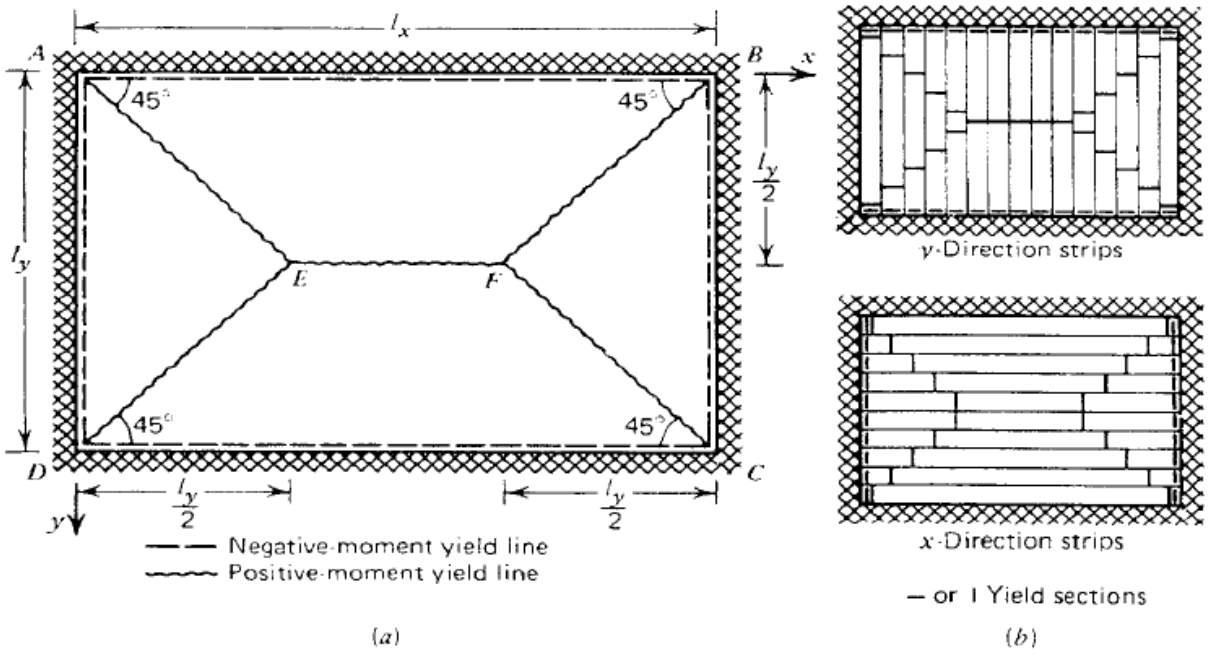

Figure 2-3. Assumed yield line and strip geometry (Park and Gamble 2000)

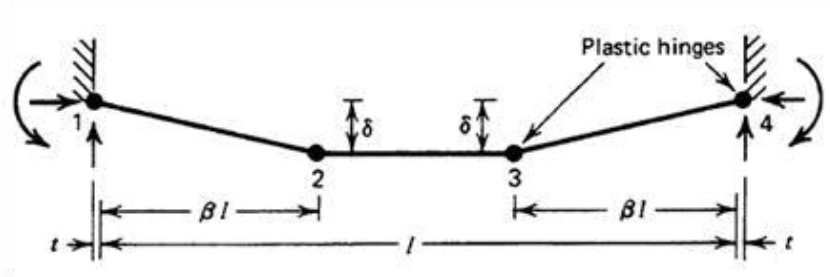

Figure 2-4. Deflections and plastic hinges of a restrained strip (Park and Gamble 2000)

The original length of the beam is l, and the lateral movement is t. The central deflection is δ, and the length between the center and end plastic hinges is βl.

The lateral movement t allows for the formation of the compression membrane forces. The locations of the plastic hinges are symmetric about the beam's center. The segments between the plastic hinges are assumed to be straight. For there to be a plastic hinge, the steel must have yielded, and the concrete must have reached its maximum strength.

Physical reality differs from this simplified diagram due to the slab's depth. This can be seen in Figure 2-5. Although the beam portions are assumed to remain straight, geometric problems arise, as portions of the slab overlap with other segments and the supports.

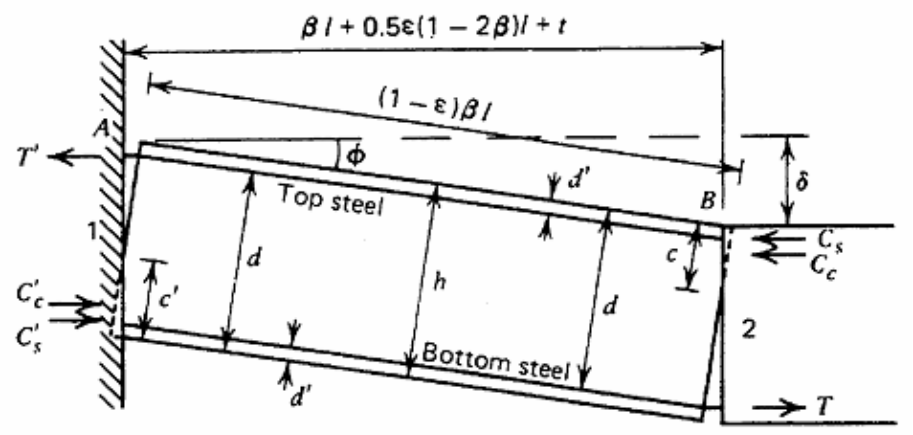

Figure 2-5. Full slab thickness between plastic hinges (Park and Gamble 2000)

From the geometry and force equilibrium in Figure 2-5, the following equations can be developed:

$$c' + c = h - \frac{\delta}{2} - \frac{\beta L^2}{2\delta}\left(\varepsilon + \frac{2t}{L}\right) \tag{2-8}$$

$$C'_c + C'_s - T' = C_c + C_s - T \tag{2-9}$$

where *c'* and *c* are the neutral axis depths for sections 1 and 2, respectively, *h* is the slab thickness, C'_c and C_c are the concrete compressive forces, C'_s and C_s are the steel compressive forces, and *T'* and *T* are the steel tensile forces.

Using the ACI equivalent rectangular stress block assumption, the compressive forces of the concrete can be calculated as

$$C_c = 0.85 f'_c \beta_1 c \tag{2-10}$$

where f'_c is the concrete's cylinder strength, and β_1 is the ratio of the depth of the ACI stress block to the depth of the neutral-axis.

The load-central deflection relationship can then be determined from the following equation from Park and Gamble (2000), which is derived using virtual work principles and the moments caused by the previous forces:

$$\frac{wl_y^2}{24}\left(3\frac{I_x}{I_y}-1\right)$$

$$= 0.8 f'_c \beta_1 h^3 \left\{ \frac{I_x}{I_y}\left(0.1 - 0.1\beta_1\right) + \left(0.4 - 0.2\beta_1\right) \right.$$

$$+ \frac{\varepsilon'_x}{1}\left(\frac{I_y}{h}\right)^2 \frac{I_x}{I_y}\left(3.5\beta_1 - 3\right) + \frac{\varepsilon'_x}{1}\left(\frac{I_y}{h}\right)^2 \left[2\frac{I_x}{I_y}\left(1.5\beta_1 - 1\right) + \left(0.5\beta_1 - 1\right) \right]$$

$$\left. - \frac{\beta_1}{1}\frac{I_x}{I_y}\left(\frac{I_y}{h}\right)^4 \left[\left(\varepsilon'_x\right)^2 \frac{I_x}{I_y} + \left(\varepsilon'_y\right)^2 \right] \right\} - \frac{1}{3.4 f'_c}\left[\left(T'_x - T_x - C'_s + C_s\right)^2 \right.$$

$$\left. + \frac{I_x}{I_y}\left(T'_y - T_y - C'_s + C_s\right)^2 \right] + \left(C'_s + C_s\right)\left(\frac{3h}{8} - d'_x\right)$$

$$+ \left(T'_x + T_x\right)\left(d_x - \frac{3h}{8}\right) + \left(C'_s + C_s\right)\left[\frac{I_x}{I_y}\left(\frac{h}{4} - d'_y\right) + \frac{h}{8}\right]$$

$$+\left(T_y^{'}+T_y\right)\left[\frac{I_x}{I_y}\left(d_y-\frac{h}{4}\right)+\frac{h}{8}\right] \tag{2-11}$$

where:

$$\varepsilon_x^{'}=\varepsilon_x+\frac{2t_x}{I_x} \tag{2-12}$$

and

$$\varepsilon_y^{'}=\varepsilon_y+\frac{2t_y}{I_y} \tag{2-13}$$

In these equations, I is the moment of inertia in the x- or y-direction, d the depth to the tension steel layer, w the distributed load on the strip and l the strip length.

External thrust applied to the outsides of the slab can enhance the compression membrane portion of the load-deflection diagram (Krauthammer 1984). Calculation of this thrust is discussed in Section 3.5.

The new thrust force, N, can then be included in the deflection diagrams and equilibrium equations above, as shown in Figure 2-6. Using these equations, the new neutral axis can be found. Calculations using the new thrust force and neutral axis can be found in Section 3.2.

This procedure is used for calculating points between B and C on the diagram. At point C, the compressive membrane forces have reached zero. Tensile membrane forces begin to develop. Figure 2-7 illustrates how these forces act. An equation was derived (Park and Gamble 2000) to calculate the relationship between load and deflection in this section of the diagram:

$$\frac{wL_y^{\,2}}{T_y\,\delta}=\frac{\pi^3}{4\sum_{n=1,3,5,\ldots}^{\infty}\frac{(-1)^{(n-1)/2}}{n^3}\left\{1-1/\mathrm{c}\quad\mathrm{o}\left(\frac{n\pi L_x}{2L_y}\sqrt{\frac{T_y}{T_x}}\right)\right\}} \tag{2-14}$$

where T_x and T_y yield forces per unit width in the x- and y-directions.

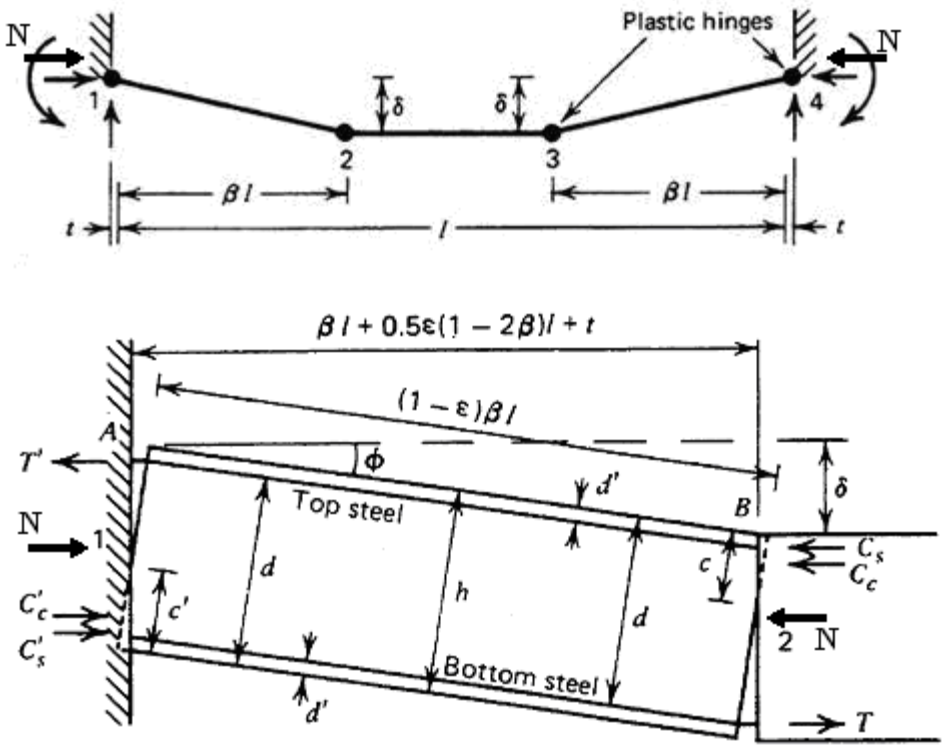

Figure 2-6. Thrust forces added to concrete strips

These aforementioned equations require there to be plastic deformations, and, therefore, large deflections. Consequently, the relationships in the early portion of the load and deflection diagrams are not addressed. A model for this segment was proposed by Krauthammer et al. (1986). Between points A and B, a quadratic function is fit. Straight lines are then used to model the portions between both points B and C, and points C and D. A drawing of this model is shown in Figure 2-8. This model uses Park and Gamble's (2000) assertions that the maximum load is reached at a deflection equal to half the slab thickness, and that the compressive membrane forces end at a deflection equal to the complete slab thickness. The accuracy of this model was verified through comparisons with experimental data.

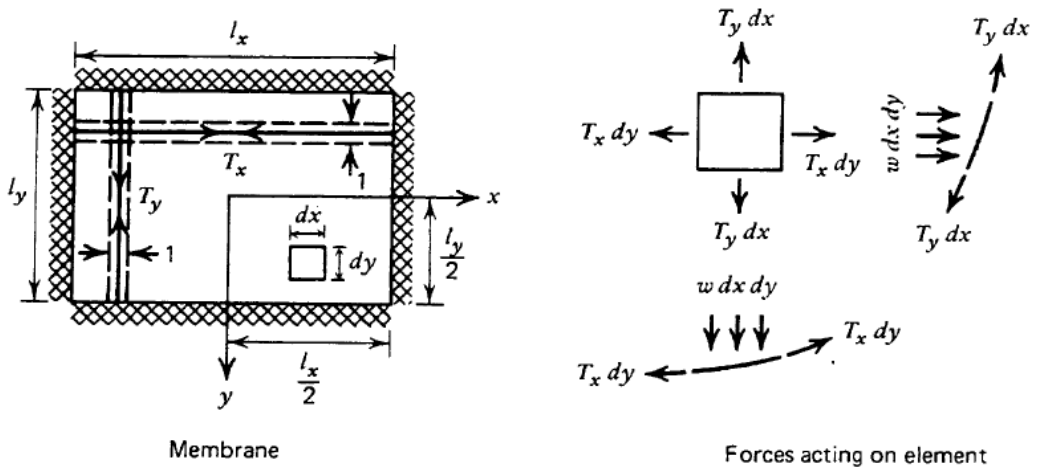

Figure 2-7. Action of tension membrane forces (Park and Gamble 2000)

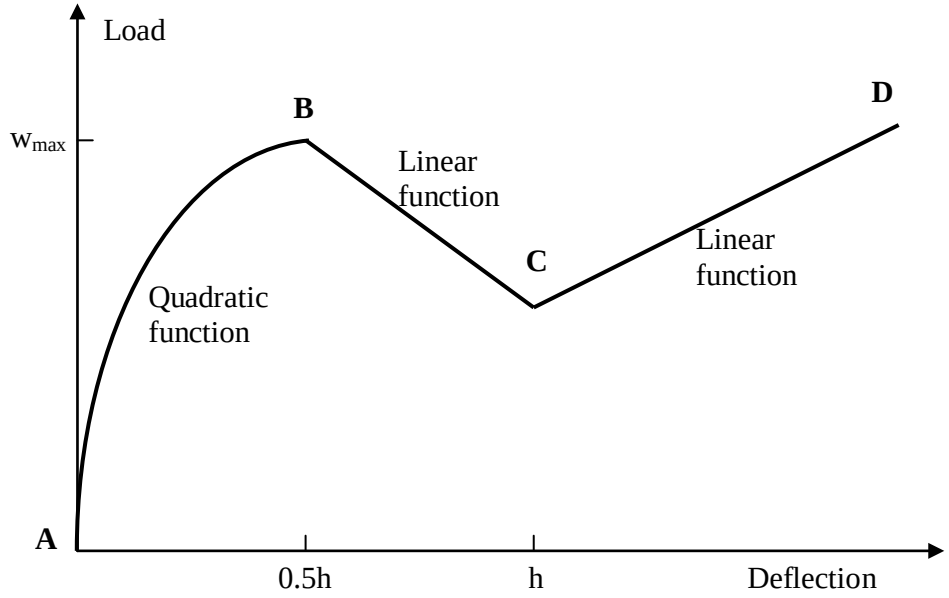

Figure 2-8. Load-deflection model for a slab (Krauthammer et al. 1986)

2.4 Direct Shear

Direct shear failure occurs through an excessive slipping along the slab's supports. When the concrete-box structure fails in direct shear, it does so in less than a few milliseconds after the load's arrival, without time to develop a significant flexural response. For this reason, the direct shear response can be uncoupled from flexural response in calculations (Krauthammer et al.

1986). Direct shear failure is of significant concern when dealing with blast loads, due to their impulsive nature.

An empirical model is used to determine the wall's response to direct shear. An earlier model developed by Hawkins (1972) was enhanced in Krauthammer et al. (1986) to take into account compression and rate effects. This was done by increasing the original model by a factor of 1.4. The original and enhanced models are shown in Figure 2-9.

The highest shear strength of the wall occurs at B' and exists through C'. Failure due to direct shear occurs at E', where maximum displacement is reached. The values of the graph points come from the following equations:

$$\tau_e = 1.6 + 0.15 f_c' \tag{2-15}$$

$$\tau_m = 8\sqrt{f_c'} + 0.8\rho_v f_{ty} \le f_c' \tag{2-16}$$

$$\tau_L = \frac{0.85 A_{sb} f_s'}{A_c} \tag{2-17}$$

$$\Delta_{max} = 2.0\left(\frac{e^x - 1}{120}\right) \tag{2-18}$$

$$x = \frac{900}{2.86\sqrt{\frac{f_c'}{d_b}}} \tag{2-19}$$

where ρ_{vt} is the ratio of total reinforcement area to the area of the plane which it crosses, d_b the bar diameter, A_{sb} the total reinforcement area, A_c the concrete cross-sectional area, f's the reinforcement's tensile strength, f_y the .reinforcement's yield strength, and ρ_{vt} the ratio of total reinforcement area to the area of the plane it crosses.

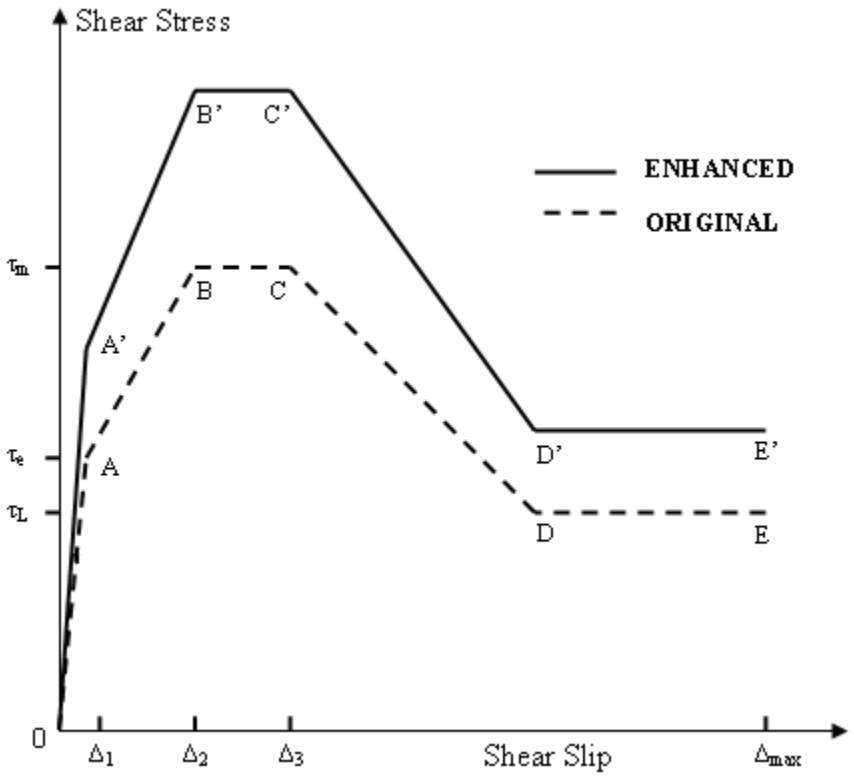

Figure 2-9. Empirical model for shear stress-slip relationship (Krauthammer et al. 1986)

2.5 Use of the Newmark-Beta Method for Integration

Even when solving simplified equations of motion, it is useful to employ a numerical evaluation method to more easily calculate the dynamic response and find a closed-form solution.

The Newmark-Beta method (Newmark et al. 1962) has been chosen for use in direct integration of the equations of motion in both the flexure and direct shear cases. The method is summarized below.

1) The equation to be used in this case is (2-1), the motion of an SDOF system:

$$F_e(t) = M_e \ddot{x} + C \dot{x} + R(x)$$

2) The values of x, $\dot{x}$, and $\ddot{x}$ are known at the initial time, $t = t_a$. The values of F_e should be known at every time, t.

3) Let $t_{i+1} = t_i + \Delta t$, where Δt is the time step.

4) A value of $\ddot{x}_{i+1}$ must be assumed.

5) Compute the values $\dot{x}_{i+1} = \dot{x}_i + (\ddot{x}_i + \ddot{x}_{i+1})\frac{\Delta t}{2}$ (2-20)

and $x_{i+1} = x_i + \dot{x}_i \Delta t + (\frac{1}{2} - \beta)\ddot{x}_i(\Delta t)^2 + \beta \ddot{x}_{i+1}(\Delta t)^2$ (2-21)

$0 \le \beta \le 1$

6) In this case, a value of 1/6 was used for β, which corresponds to a parabolic variation.

7) By inputting these new values into the original equation of motion, (2-1), compute a new value for $\ddot{x}_{i+1}$.

8) Repeat steps 5 and 7 with the new values of $\ddot{x}_{i+1}$ until a convergent value is reached.

9) Repeat the process for the next time step.

10) The method starts at time $t = 0$, the time when the load is first applied. The system is initially at rest, so $x = \dot{x}_i = 0$ and $\ddot{x}_0 = \frac{F(0)}{m}$.

2.6 Underground Blasts

2.6.1 Ground Shock

A blast taking place below the ground surface behaves differently than a blast in the open air. In an explosive event occurring in the open air, the explosion pushes air away, creating a vacuum. Once the pressure is gone, air flows back into this vacuum, creating a negative pressure phase. This does not occur in soils. Instead, the blast pushes on the soil and creates a crater, which may eventually be filled by soil due to gravity effects. There is no negative

pressure phase. An underground explosion usually generates a greater stress and has a longer duration than if that same explosion were to occur in air (ESL-TR-87-57 1989). Therefore, its impulse will be much greater.

When detonation occurs, the intense pressure wave caused by expanding gasses at areas close to the blast creates stress waves in the soil and crushes air voids present in the soil, creating a crater or cavity. Initially, these gasses are very hot, but they cool as this new, expanding soil cavity is being formed. As the gasses cool, their volume decreases, resulting in relief or unloading waves, similar to the suction pressures in an air blast. Since the soil through which these relief waves travel has been densified by the initial stress waves, they travel faster than the initial waves did, and eventually overtake them. In doing so, they attenuate the intensity of the shock front. To account for this in calculations, an attenuation coefficient is included, though only a rough estimation. Soils where this attenuation occurs more quickly have a low relative density or a large percentage of air voids. Conversely, soils with a high relative density or a low percentage of air voids will attenuate the ground shock much more slowly.

Saturation in soils can also affect the shock transmission. Water can fill air voids and increase a soil's density. In cohesive soils, as saturation approaches 100 percent, the peak pressure and stress transmissions begin to behave like they would in water. In saturated granular soils with low relative densities, it is possible for the pressure wave to collapse the soil skeleton, liquefying the sand. These types of granular soils are not recommended for use in the construction of buried facilities (ESL-TR-87-57 1989).

Since a pressure wave expands spherically after an explosion, the pressure at any point is proportional to a ratio of the range of this point to the cube root of the charge weight. This is

known as the scaled distance, and the validity of its use in buried explosives has been proven using 35 years of explosion data.

Using this scaled distance and attenuation coefficient, an equation was created for the calculation of the peak free-field pressure in the soil at a given distance from the explosion:

$$P_0 = \frac{1}{1}\frac{6}{4}\frac{0}{4} f c \rho_0 \left(\frac{R}{W^{\frac{1}{3}}} \right)^{-n} \tag{2-22}$$

Here, P_0 is the peak free-field pressure (psi), c the seismic velocity of the soil (ft/s), ρ_0 the soil density (lb/ft^3), R the range (ft), W the charge weight (equivalent weight in lbs of C4), n the attenuation coefficient (unitless), and f (unitless) the coupling factor. A basic sketch of an underground blast pressure-time history is shown in Figure 2-10.

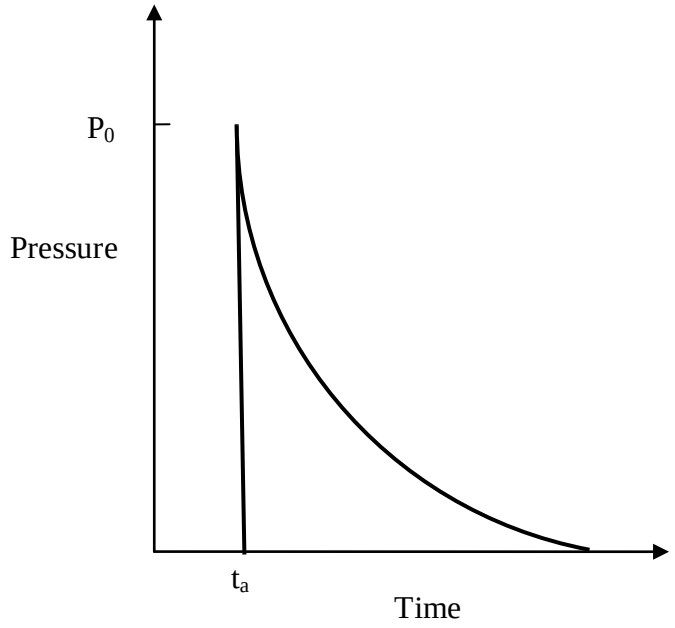

Figure 2-10. Sketch of an underground blast pressure-time history

After the arrival of the pressure wave, the pressure at any given time can be calculated from the following equations:

$$P(t) = P_0 e^{-\alpha(t-t_a)} \tag{2-23}$$

$$t_a = \frac{R}{c} \tag{2-24}$$

$$\alpha \approx \frac{c}{R} \tag{2-25}$$

where, t_a is the arrival time (seconds).

The relevant duration of the blast load recommended for use in these equations is approximately four times the arrival time. The use of a linear rise is recommended in place of an instantaneous rise to the peak pressure at its arrival time. The duration of this recommended linear rise is one tenth of the arrival time (ESL-TR-87-57 1989).

The coupling factor, *f*, reflects how much of the blast's energy has been coupled into the soil, as opposed to being lost into the air, etc. at the ground's surface. This value can be interpreted off of the graph in Figure 2-11.

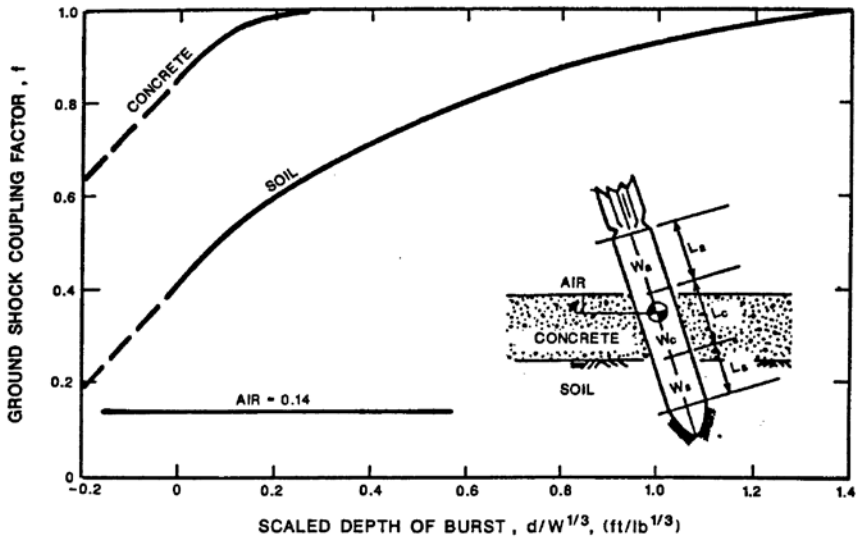

Figure 2-11. Ground shock coupling factor as a function of scaled depth (ESL-TR-87-57 1989)

2.6.2 Soil Arching

Soil arching is a process in which the shear strength properties of a soil can favorably redistribute a load applied to a buried structure (ASCE 1985). When a uniform load is applied to

a face of a buried structure, and it responds flexurally, the soil may passively redistribute the load away from the center of the wall. Through strong shear forces, the load is directed away from the retreating wall and sent towards the stationary portions of the system. This includes the outer walls of the box and surrounding soil, where the load will be less damaging to the structure.

The effects of soil arching will not be including in this study for two reasons. First, it is often ignored for purposes of a conservative design approach (ASCE 1985). Second, soil arching is a process where a uniform load becomes redistributed; the load from an underground blast is not uniformly applied to the structure. The blast will be spherical, resulting in higher loads at the central portion of the wall and decreasing loads toward the outer edges. It is possible that this load distribution will counteract the effects of soil arching.

2.7 One-Dimensional Elastic Wave Behavior

Elastic wave behavior is the simplest option for use in predicting the pressure waves' actions at material interfaces, including between soil layers, at the soil surface, and at the boundaries between the box and soil. This is an approximation, however, because the attenuated pressure waves may behave as elastic waves, but the pressure waves near a buried explosion do not. The material recovers back to its undisturbed state once an elastic wave has passed; no plastic deformation has occurred.

The propagation of an elastic wave is defined by the dynamic equilibrium equation:

$$\sum F = ma \tag{2-26}$$

Inputting the forces, masses, and acceleration in a small, one-dimensional length of the solid, δx, yields the following equation:

$$\rho A \delta x \frac{\partial^2 u}{\partial t^2} = A \partial x \frac{\partial \sigma}{\partial x} \tag{2-27}$$

where ρ is the solid's density, A the cross-sectional area of the volume being investigated, u the particle velocity, σ stress, x the direction of travel, and t time.

Simplifying this equation and applying Hooke's Law yields:

$$\rho \frac{\partial^2 u}{\partial t^2} = E \frac{\partial^2 u}{\partial x^2} \tag{2-28}$$

where E is the material's modulus of elasticity.

By simplifying this equation, the elastic wave velocity in any solid can be found:

$$c = \sqrt{\frac{E}{\rho}} \tag{2-29}$$

where c is the wave velocity.

Each material has its own elastic wave velocity. For example, the elastic wave velocity in concrete is around 10,000 ft/s. In soils, elastic wave velocity is more commonly referred to as seismic velocity.

When an elastic wave traveling through one medium encounters the boundary with another medium, including air, a portion of the stress wave will be transmitted into this new medium, and a portion will be reflected back into the original medium. At these interfaces, there is assumed to be continuity in both normal stress and displacement, resulting in an equality of velocity. The interface is assumed to remain stationary, and the materials are assumed to remain in contact. From these assumptions, the following equilibrium equations can be applied at the boundary:

$$\sigma_I + \sigma_R = \sigma_T \tag{2-30}$$

$$\dot{u}_I + \dot{u}_R = \dot{u}_T \tag{2-31}$$

$$u_I + u_R = u_T \tag{2-32}$$

where σ is the normal stress, $\dot{u}$ is the normal particle velocity, and u the normal particle displacement. I, R, and T indicate incident, reflected, and transmitted, respectively.

Stress and particle velocity are related by the following equation:

$$\sigma = \rho c \dot{u} \tag{2-33}$$

Using these equations, equations to calculate the values for actual stresses transmitted and reflected can be derived:

$$\sigma_T = \sigma_I \frac{2\rho_2 c_2}{\rho_1 c_1 + \rho_2 c_2} \tag{2-34}$$

$$\sigma_R = \sigma_I \frac{\rho_2 c_2 - \rho_1 c_1}{\rho_1 c_1 + \rho_2 c_2} \tag{2-35}$$

where 1 and 2 indicate the initial and newly encountered media, respectively (Tedesco 1999).

Depending on the material properties, it is possible for the reflected wave to have a different sign than the incident wave. As the density of the second medium approaches zero, as is assumed with air, the reflected wave approaches the full intensity of the incident wave, but with the opposite sign. As the density of the second medium approaches infinity, the reflected wave approaches the full intensity of the incident wave, with the same sign (Tedesco 1999).

It is possible that the wave itself will not be traveling in a direction normal to the boundary. In this case, it is important to be able to calculate the direction of the new waves. The reflected wave will rebound at the same angle as the incident angle. The transmitted wave will have the same normal wave velocity as the incident wave. Having different elastic wave velocities, they will have different directions of travel. This is illustrated in Figure 2-12. Using trigonometry, these angles can be found from the following equation:

$$c_1 \cos(\theta_1) = c_2 \cos(\theta_2) \tag{2-36}$$

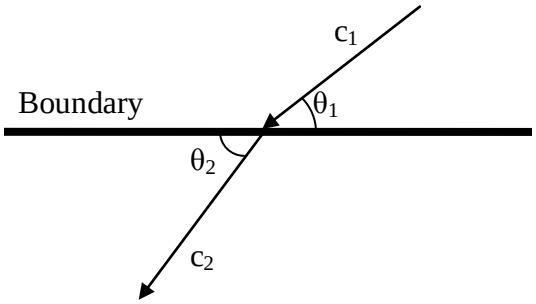

Figure 2-12. Change in direction after a wave transmission

2.8 Summary

In this chapter, the behavior of the wall of a concrete box, as well as methods for estimating this behavior using SDOF systems, was first discussed. This discussion focused on flexure and direct shear behavior, the most likely failure modes for the wall of a buried concrete box subjected to the effects of a buried HE explosive. The numerical method for integration was then discussed. The effects of a buried explosive on soil were also presented, as well as the behavior of elastic wave propagation.

The background presented in this chapter sets the foundation for the methodology discussed in the following chapter.

CHAPTER 3
METHODOLOGY

3.1 Introduction

Using the material behaviors discussed in the previous chapter, methods for calculating loads on the structure and the structural response can be formulated.

This chapter discusses the methodology used in creating the resistance functions for both flexural and direct shear responses for the wall of an RC box, in Sections 3.2 and 3.3, respectively. The methods used in the creation of the load and the thrust created by the load are discussed in Sections 3.4 and 3.5, respectively. Flow charts of the procedures as included in DSAS are located in Section 3.6.

3.2 Flexural Response

As mentioned in Section 2.3, modifications need to be made to values on the load-deflection diagram (Figure 2-2) to account for the compression membrane forces enhanced by the external thrust. To determine this new flexural resistance, calculations begin by dividing unit widths of the concrete slab into a series of layers, as illustrated in Figure 3-1. The stresses in each layer are then determined individually, using the chosen stress-strain relationships: the Hognestad model (MacGregor and Wight 2005) for concrete, and the Krauthammer and Hall (1982) model for steel. Once the resulting total force and moment about the neutral axis, n_u and m_u, respectively, have been calculated, the wall's deflection can be found by equating the internal work done by these values to the external work done by the blast load. This process is used for points B and C, where the deflections have been assumed as equal to one-half the slab's depth and the full slab depth, respectively. Then a linear function can be fit between the two points. The value at point B should be a local maximum, and compression membrane forces should no longer be present at point C.

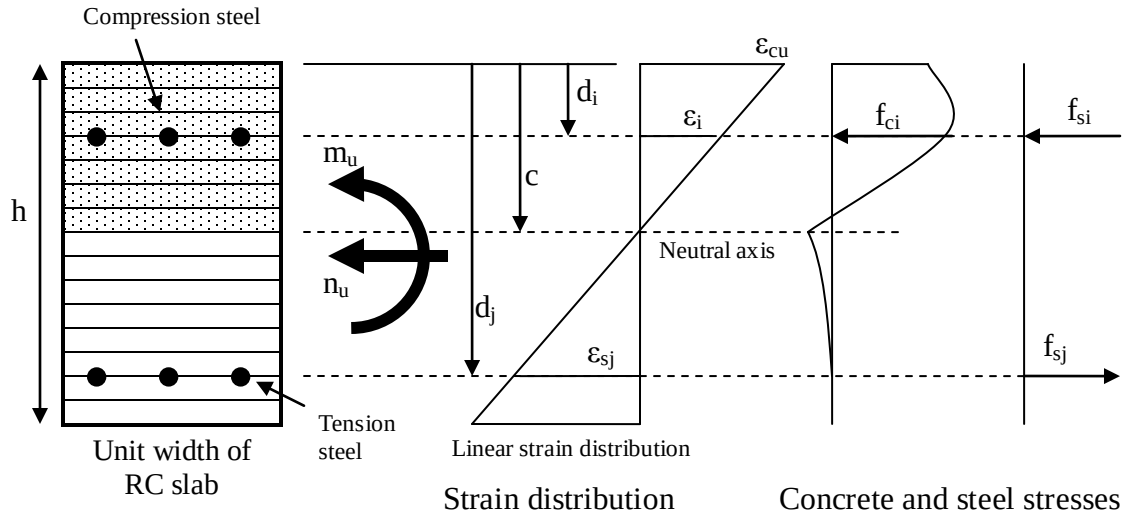

Figure 3-1. Unit width divided into layers and corresponding stress distributions

As evident from the figure, n_u and m_u are functions of the neutral axis depth, c. These apply to the central portion of the slab, between the middle plastic hinges. The same holds true for the corresponding forces n_u' and m_u', which are functions of their neutral axis depth, c'.

The strains in the concrete and steel at each of their layers can be calculated from the following equation, derived from the geometry of the strain distribution:

$$\varepsilon_i = \frac{\varepsilon_{cu}}{c}\left(c - d_i\right) \tag{3-1}$$

where ε_i is the steel and/or concrete strain in the layer, ε_{cu} the ultimate concrete strain at its failure, d_i the depth to the layer, and c the neutral axis depth. The stresses in each of these layers, f_i, can then be determined from the materials' stress-strain diagrams.

These strains can then be converted into forces, and the forces can be used to calculate the total section moment and axial force, as shown in the following equations:

$$F_i = f_i A_i \tag{3-2}$$

$$m_u = \sum_{i=1}^{\#\ layers} F_i\left(\frac{h}{2} - d_i\right) \tag{3-3}$$

$$n_u = \sum_{i=1}^{\#\ layers} F_i \tag{3-4}$$

where F_i is the steel and/or concrete layer force, A_i the area of the layer, h the slab thickness, m_u the total section moment, and n_u the total section axial force.

Based on deformation geometry, the strain and movement portion of equation (2-8) can be determined as follows:

$$\left(\varepsilon + \frac{2t}{L}\right) = \frac{n_u}{hE_c} + \frac{2(n_u - N)}{LS} = \varepsilon_{total} \tag{3-5}$$

where E_c is the elastic modulus of the concrete, S the surround stiffness, and N the thrust force.

By substituting equation (3-9) into equation (2-8), it can be written as a function of the neutral axis depths c and c', as can the equilibrium of membrane forces:

$$R_1(c,c') = c' + c - h + \frac{\delta}{2} + \frac{\beta L^2}{2\delta}\left(\frac{n_u}{hE_c} + \frac{2(n_u - N)}{LS}\right) = 0 \tag{3-6}$$

$$R_2(c,c') = n_u - n_u' = 0 \tag{3-7}$$

Through iteration, values of c and c' at any displacement value, δ, can be found from equations (3-6) and (3-7). These values of c and c' can then be used in equations (3-3) and (3-4) to find the total values of n_u, m_u, and m_u' in each strip, for use in virtual work calculations.

As mentioned in Chapter 2, in order to use an SDOF system approximation, factors need to be applied to the total load and mass. Since a range of factors are listed in Biggs (1964), dependent on the behavior of the material (elastic, plastic, etc), it was decided to use different factors throughout the course of the load-deflection diagram. Initially, at point A, the behavior is elastic. Between points A and B, the factors are varied linearly to elastic-plastic first, and then to plastic at B. From B to C, the values go from plastic to the tension membrane values. These tension membrane values are then used from point C through D. This is illustrated in Figure 3-2.

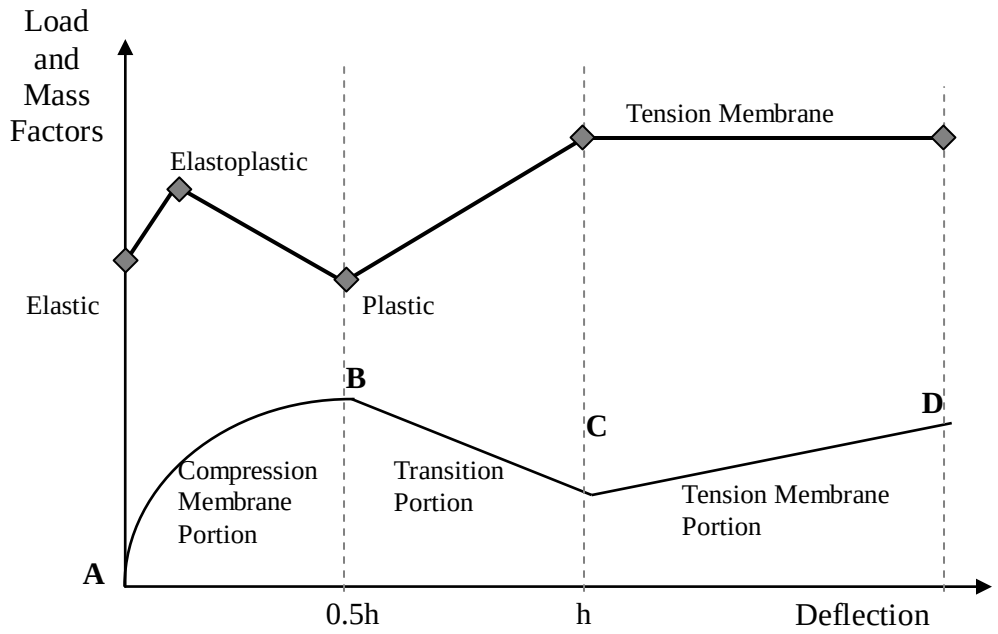

Figure 3-2. Variation of load and mass factors

The factors for elastic, plastic and elastoplastic portions can be found in Biggs (1964), but the tension membrane factors must be calculated using the methods discuss in Section 2.2. During the tension membrane portion of its response, a beam with a uniform load applied is assumed to have a parabolic deformed shape, defined by the following equation:

$$\phi(x) = \frac{4}{L}x - \frac{4x^2}{L^2} \qquad \text{for } 0 \le x \le L \tag{3-8}$$

Inputting this value into equations (2-4) and (2-7):

$$K_M = \frac{M_e}{M_t} = \frac{\int_0^L m\phi^2(x)\,dx}{mL} = \frac{\int_0^L \left(\frac{4}{L}x - \frac{4x^2}{L^2}\right)^2 dx}{L} \tag{3-9}$$

$$K_M = \frac{8}{15} = 0.533$$

$$K_L = \frac{F_e}{F_t} = \frac{\int_0^L p(x)\phi(x)\,dx}{p(x)L} = \frac{p(x)\int_0^L \left(\frac{4}{L}x - \frac{4x^2}{L^2}\right)dx}{p(x)\ L} \tag{3-10}$$

$$K_L = \frac{2}{3} = 0.667$$

These equations correspond to the unit width (treated as a beam) of a one-way slab. The same approach can be used for calculating the factors for a two-way slab.

3.3 Direct Shear

The basic concepts and load-deflection curves used in direct shear calculations were discussed in Chapter 2. These concepts apply to one-way slabs, but modifications must be made for their use with two-way slabs. The x- and y-directions can be looked at separately, as shown in the following equations:

$$M_{ex}\,\ddot{w}_x + C_x\,\dot{w}_x + R_x(w) = V_{ex}(t) \tag{3-11}$$

$$M_{ey}\,\ddot{w}_y + C_y\,\dot{w}_y + R_y(w) = V_{ey}(t) \tag{3-12}$$

where *w* is the degree of freedom, i.e. the slip of the slab, and the forcing function is *V*, a shear force.

Since the slab is assumed to not flex, it can be treated as a single moving mass. Therefore, the x- and y-directions both experience the same slab displacement, *w*. Equations (3-11) and (3-12) can then be combined as follows:

$$\left(M_{ex} + M_{ey}\right)\ddot{w} + \left(C_X + C_y\right)\dot{w} + \left(R_x(w) + R_y(w)\right) = \left(V_x(t) + V_y(t)\right)$$

$$M_{e,total}\,\ddot{w} + C_{total}\,\dot{w} + R_{total} = V_{e,total}(t) \tag{3-13}$$

In two-way slabs, the resistance can be assumed as the sum of the resistances in the x- and y-directions. In addition, due to the simple deformed shape, the load and mass factors can be taken as 1.0. The equivalent mass is the total slab mass, and the equivalent load is the total shear load on the slab. The resistance is the sum of the resistances around the support perimeter.

3.4 Load Function Creation

To treat the wall of the RC box as an SDOF system, a single forcing function must be applied. Since an underground blast does not create a uniform load on the wall, an average force from the whole wall must be created.

In this section, first the blast wave reflections and transmissions are discussed, then the conversion from free-field pressures to a wall surface pressure is explained. Lastly, the techniques used in creating an average pressure on the wall are discussed.

3.4.1 Soil Layer Reflections and Transmissions

The existence of dense soil layers can increase the load on the wall by reflecting additional pressure waves back towards the wall, as discussed in Section 2.7. Waves reflecting from the ground's surface or a less dense layer may also send a negative pressure wave, reducing the load on the wall. All of these additional reflected pressures must be accounted for when calculating the total load on the wall.

The values of these pressure waves can be calculated using a combination of the pressure equations found in Section 2.6 and the reflection and transmission coefficients found in Section 2.7. First, the maximum pressure is calculated using equation (2-22), this is then multiplied by the reflection and/or transmission equations (2-34) and (2-35) as necessary, dependent upon the number of times the wave has been reflected or transmitted before reaching the wall. Equations (2-23) through (2-25) can then be used in conjunction with this newly-modified peak pressure to develop a pressure-time history of the reflected wave. The soil weight and wave speed to be used in these calculations are the density and wave speed of the soil in which the wall is located, since these will be the final speed of the wave as it reaches the wall and the density of the soil that will be pressing on the wall.

It may be difficult to calculate the range of a wave which has been transmitted through an additional layer because, as shown in Figure 2-12, the wave will change direction. The true range is the sum of the total distances traveled by the wave, so these changes in direction must be accounted for. In order to simplify this, the soil layers can be artificially stretched or compressed so that the same wave speed can be used in calculations. The wave will still have the same arrival time, but there will be no change in direction at the interfaces, allowing for a simpler calculation of range. The equation used to artificially change a layer's depth is shown below:

$$d_{new} = d \frac{c_{blast\_layer}}{c_{current\_layer}} \tag{3-14}$$

where d is the layer depth. This layer resizing is illustrated in Figure 3-3.

Another way to simplify the reflection and transmission calculations is to consider each as its own direct pressure wave coming from a new source, rather than as a reflection emanating from the original explosive charge. These new charges are located directly above or below the charge in such a way that their direct pressure wave would travel for the same amount of time as the reflected/transmitted waves, but never change direction. The reflection and transmission coefficients still apply. In relation to the original charge itself, only the pressure-time history of the direct pressure wave would be considered. All of these individual pressure-time histories can then be summed to get a total pressure-time history at a point. The use of these new charges is illustrated in Figure 3-3.

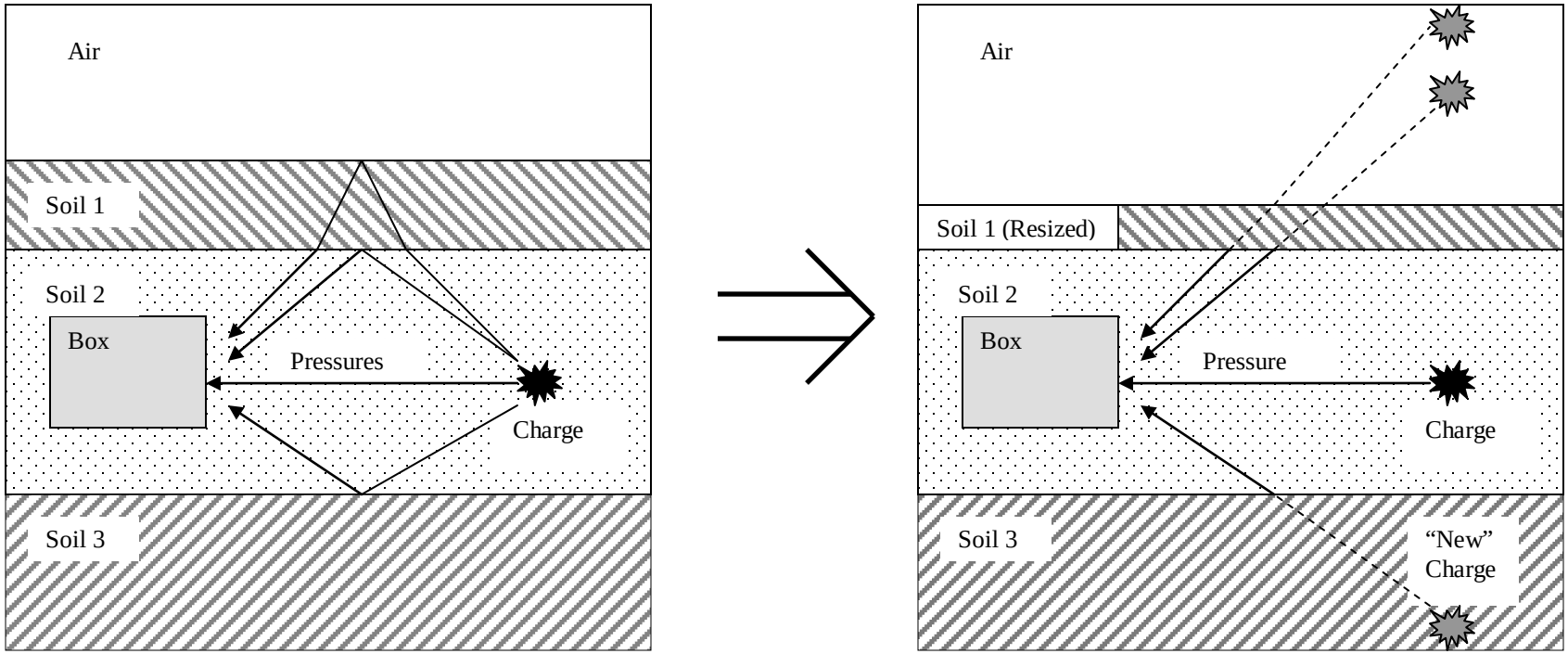

Figure 3-3. Illustration of simplification used in reflected and transmitted wave calculations, including soil layer resizing and investigating each pressure wave as coming directly from its own charge

3.4.2 Converting Free Field Soil Pressure to an Interface Pressure

The equations presented in Section 2.6 and expanded upon in other portions of this paper only calculate the free-field pressures in soil. This is different from the pressure felt on a surface. In order to find this surface pressure, elastic wave reflection is again used. The pressure on the wall is the sum of the free-field pressure and the force of reflecting the wave back. Once all the free-field pressures, both direct and from reflections, have been calculated, the surface pressure can be calculated using the following equations:

$$P_{wall}(t) = (1 + r) * P(t) \tag{3-15}$$

$$r = \frac{\rho_{concrete} c_{concrete} - \rho_{soil} c_{soil}}{\rho_{concrete} c_{concrete} + \rho_{soil} c_{soil}} \tag{3-16}$$

where $P_{wall}(t)$ is the pressure on the wall and $P(t)$ is the original total of all free-field pressures. Equation (3-16) is a modification of equation (2-35), specifically for use with soils and concrete.

3.4.3 Calculating Average Pressure

The pressure equations discussed earlier can only calculate a pressure-time history at one single point. Taking only the pressure on the center point of the wall would overestimate the wall's loading; an average pressure on the wall's surface must be created for use in the SDOF calculations.

It was originally determined to divide the entire wall into a grid of one hundred rectangles, ten rectangles vertically by ten horizontally. This is illustrated in Figure 3-4. Ten was chosen to allow for simple divisions. The time-dependent pressure equations could then be found at the center of each rectangle. By averaging these pressures and multiplying by the area of the rectangle, an average force could be obtained. This average force could then be converted to a uniform load on the wall. However, since the pressure equations are continuous in respect to time, a finite number of times would need to be used in order to have values to average.

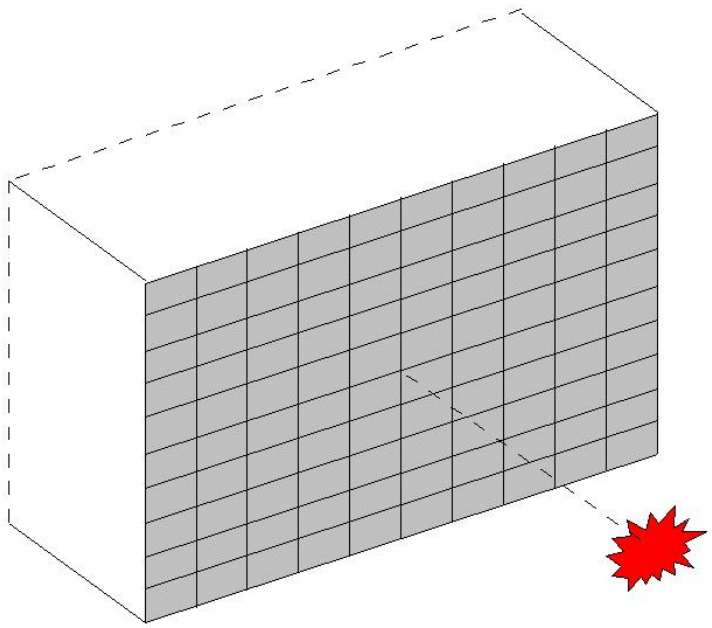

Figure 3-4. Original design for a 10 x 10 rectangular grid across the entire wall

The duration of the entire loading on the structure begins at the start of the rise of the first pressure to reach the wall. It ends at the end of the duration of the last pressure to reach the wall. As mentioned in Section 2.6, the duration of one pressure-time history was estimated as four times its arrival time. The overall duration was then divided into a number of time steps. Then, at each of step, the time was put into the one hundred rectangles' pressure equations, and a total pressure was found.

It was discovered that using the average pressure over the entire wall resulted in a greatly underestimated load. Since the outer portion of the box would take not feel any pressure until much later, many rectangular areas were contributing a zero pressure to the average while the wall's center, the most important section and the section most affected by flexure, was experiencing its greatest load.

It was decided that instead of taking an average pressure over the entire wall, the new force would come from a square area of the wall nearest to the charge. This square would be as large as the height of the box, and have the charge located at its center. In this way, the portions

of the box experiencing very little pressure, which also experience the least deflection, would not distort the averages. The square layout is illustrated in Figure 3-5.

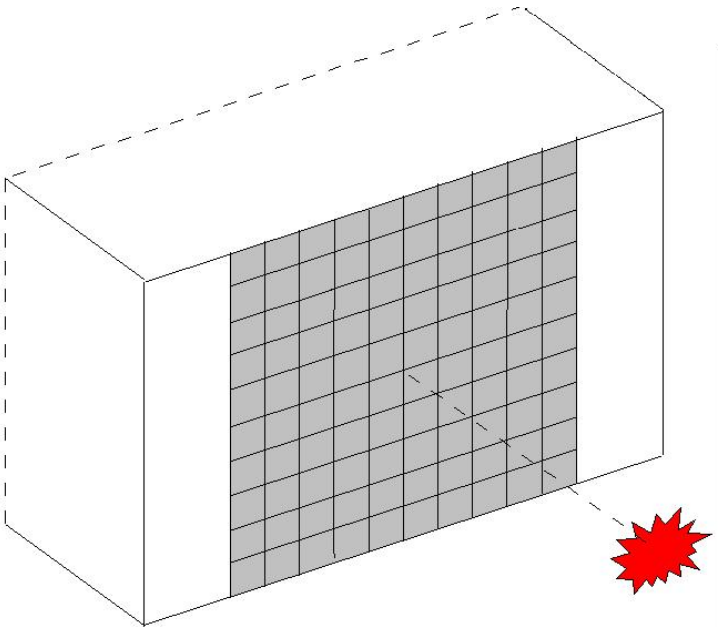

Figure 3-5. Modified square 10 x 10 grid nearest to the explosion

3.5 Thrust

As mentioned in Section 2.3, the external thrust must be taken into account when creating the wall's resistance functions. By increasing compression membrane forces, these axial forces can increase the ultimate load that a wall or slab can resist. A method had to be formed to calculate these thrusts, having calculated the forcing function.

This thrust is created by the pressure wave as it travels across the surfaces of the box (the sides, top, and base), and applies a load to all of these faces. These loads are then transmitted to the ends of these sides, where they create axial forces on the adjoining walls.

To calculate the values of these thrust forces, unit-width strips at the box's roof, base, and one side are used. As the pressure wave travels across one of these strips, the load it applies is dependent upon the coefficient of lateral earth pressure, a soil property that determines how much force applied to a soil in one direction will be felt in perpendicular directions. The

pressure wave's strength continues to dissipate due to the increase in range from the explosive, as discussed in Section 2.6. The coefficient of lateral earth pressure is so named because it was originally used to determine what kind of lateral force, due only to a soil's weight, would be applied to a vertical wall meant to hold back a volume of soil. It can be calculated from the following equation:

$$K_0 = 1 - \sin(\phi) \tag{3-17}$$

where K_0 is the coefficient of lateral earth pressure and ϕ is the soil's friction angle.

The thrust on the wall is calculated from the reactions of the strips in the adjoining members, assuming the strips are simply supported. The load on the face of the structure at each time step over the entire explosive event is already known before the thrust function is calculated. At each time step, the following procedure is performed to calculate the thrust:

1) The load applied to the wall facing the blast is multiplied by K_0 and applied at the very end of the unit-width strip.
2) Any load points already on the unit-width strip are moved down a distance equal to the time step multiplied by the soil's seismic velocity. They are also decreased in magnitude by this increase in range. Should any of these points move beyond the end of the box, they are ignored.
3) The areas between these load points are taken as trapezoidal distributed loads. Using the areas of these trapezoids, the locations of their centroids, and the summation of moments, the reaction forces are calculated.
4) The inverse of the reaction force at the end of the strip corresponding to the wall being analyzed is the thrust force.

A portion of this thrust method is illustrated in Figure 3-6.

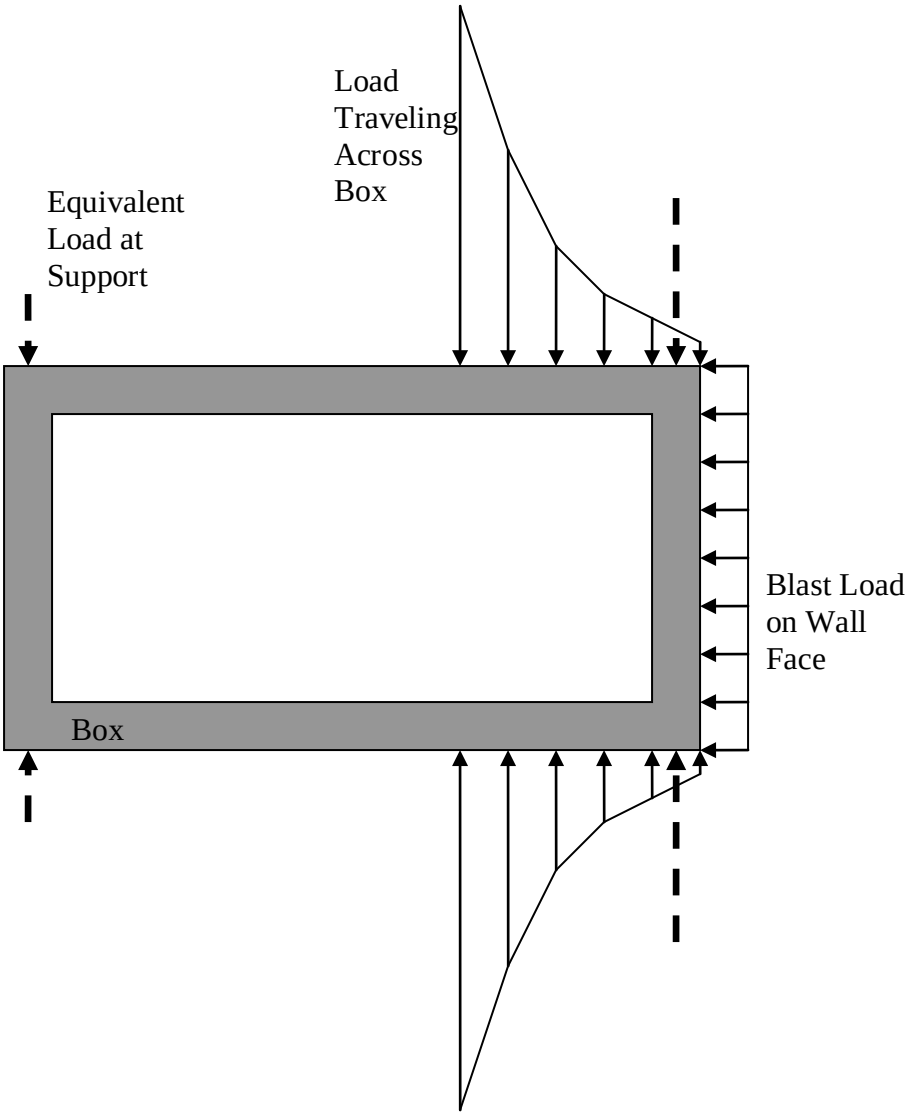

Figure 3-6. Distributed trapezoidal forces creating thrust loads

The roof, base, and one side wall are each analyzed separately due to the possibility of there being different soils present, and, therefore, the possibility of different coefficients of lateral earth pressure and seismic velocities. For example, the box may have been built or placed on a denser soil and then backfilled with a less dense material, resulting in a different soil along the box's base. For this reason, two separate resistance functions are also used, one for the horizontal direction and one for the vertical. For the horizontal direction, the thrust on one side

of the box was used in calculating the resistance function; for the vertical, an average thrust from the roof and base was used.

3.6 Program Flowcharts

A flowchart outlining the order of the procedures performed by DSAS to analyze the effects of an explosive on the wall of a buried RC box structure is shown in Figure 3-7. Figure 3-8 provides a flowchart expanding upon the load function generation of the program.

In the main program, after all parameters have been input, the load function is calculated first. From this, the thrust can then be calculated. Two SDOF systems are then run to analyze the wall response: one for calculating flexural response and one for calculating direct shear response. For flexural response calculations, the resistance function must be recalculated at each time step due to the change of the thrust force.

The load function generating portion of the program begins by artificially stretching the soil layers so as to use only the seismic velocity of the layer in which the box is located. The square portion of the wall nearest to the charge is then divided into a ten by ten grid, with the location of the center of each grid box known. Additional charges, representing the source locations of reflected and transmitted waves, are then created. The arrival and departure times for the load on the entire box wall are then calculated. At each time step between the arrival and departure times, the loads on each rectangle are calculated and averaged to create the average load on the box.

3.7 Summary

In this chapter, the methodology used in creating both the loads and the resistance functions was discussed, allowing for the calculation of the buried RC box wall's reaction to an underground blast. These methods were coded into a portion of the computer program DSAS

and tested against existing experimental data. The results of these comparisons can be found in the next chapter.

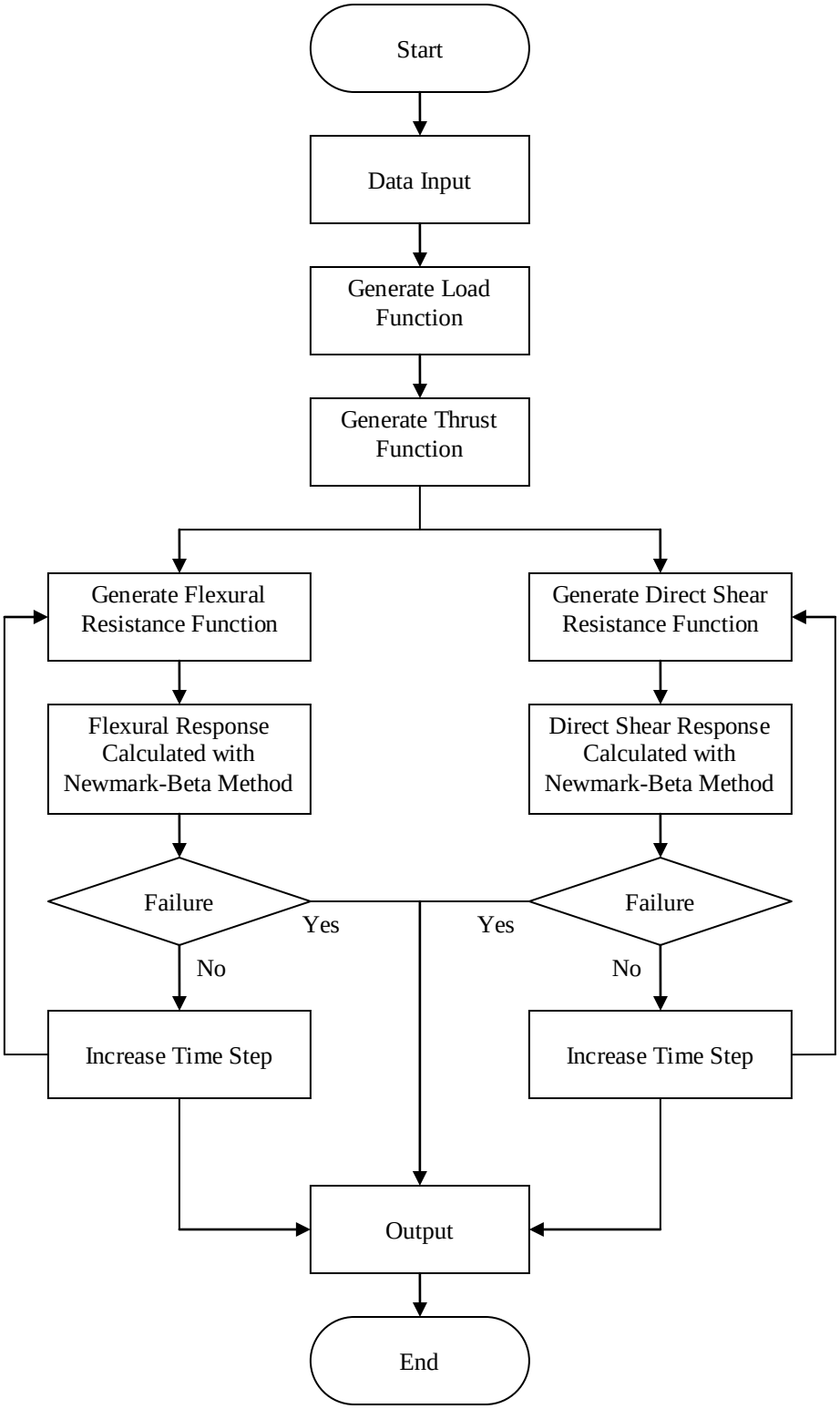

Figure 3-7. Program flowchart

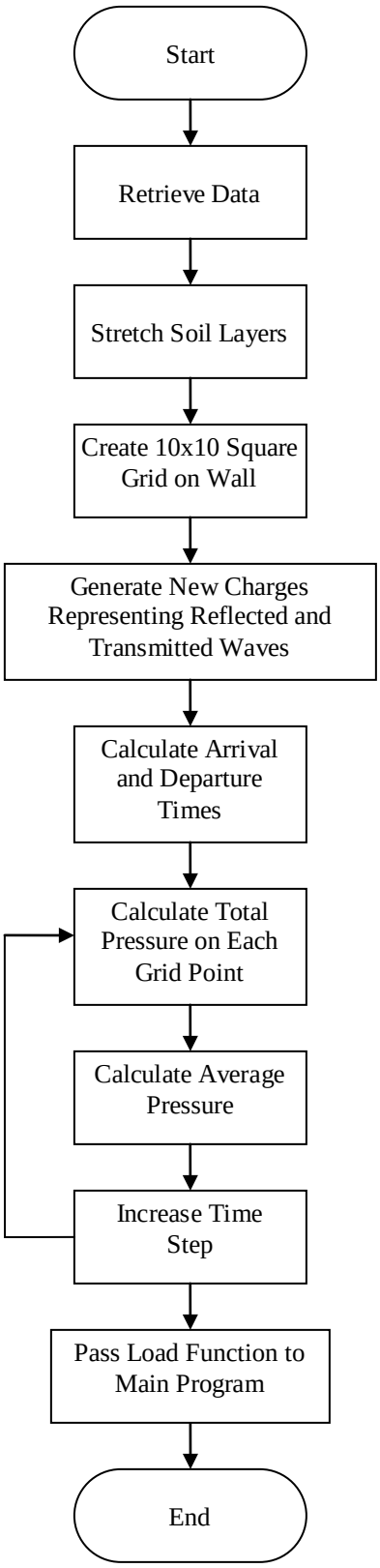

Figure 3-8. Load function flowchart

CHAPTER 4
RESULTS AND DISCUSSION

4.1 Introduction

The procedures proposed in Chapter 3 were coded into the computer program Dynamic Structural Analysis Suite (DSAS) in order to validate their results. Pressure and damage data from an existing experiment performed by Kiger and Albritton (1980), subjecting buried boxes to buried explosives, was used to validate the proposed methods for generating resistance models for a box. This pressure data was also used to determine the validity of the proposed methods for calculating loads. Intermediate portions of pressure calculations were compared with those from the existing computer program ConWep (Hyde 1992), to verify that they indicated similar results.

4.2 Box Validation Using Experimental Data

The Kiger and Albritton (1980) tests involved the burial of two box structures, known as 3C and 3D. A number of charges of an equivalent weight were buried and detonated at predetermined points around either of these boxes. The size of the explosives used is detailed in their report. More details on the boxes, site, and test conditions can be found in the Appendix.

Pressure-time histories on the box surface were recorded for five of these detonations, referred to as "shots," two from box 3C and three from box 3D. The make-up of these boxes, along with their recorded load functions, was put into DSAS to test the flexure and direct shear resistance functions. Damping ratios of 20% for flexure and 5% for direct shear were used. The higher damping ratio in the flexural case was meant to account for energy dissipation caused by soil-structure interaction (Krauthammer et al. 1986). Calculated displacements were then equated to a possible damage level and compared to the observed damage. The means of doing so, as well as the data comparison, can be found in the next sections.

4.2.1 Box Resistance Models

From the properties entered, DSAS calculated equivalent resistance models for each box. Examples of the flexural and direct shear resistance models that were generated by the program are shown in Figures 4-1 and 4-2. Information on the dimensions, material properties, and rebar layouts used in both boxes is located in the Appendix.

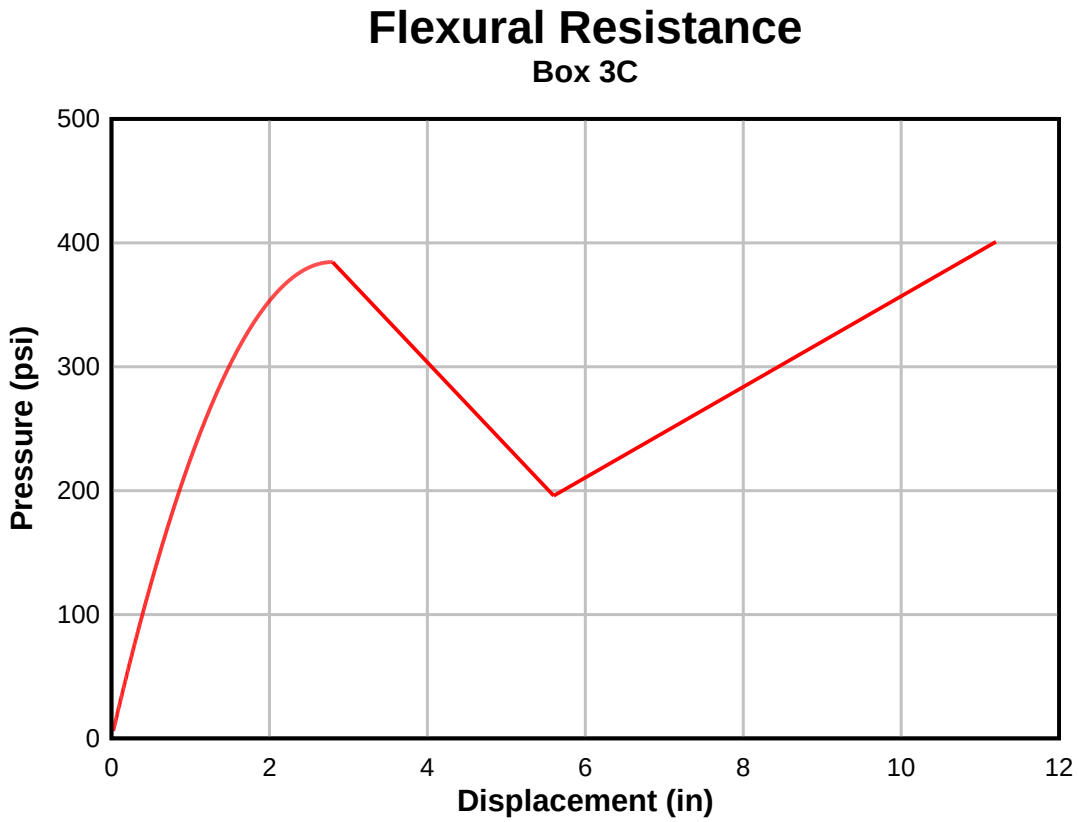

Figure 4-1. Flexural resistance model for box 3C

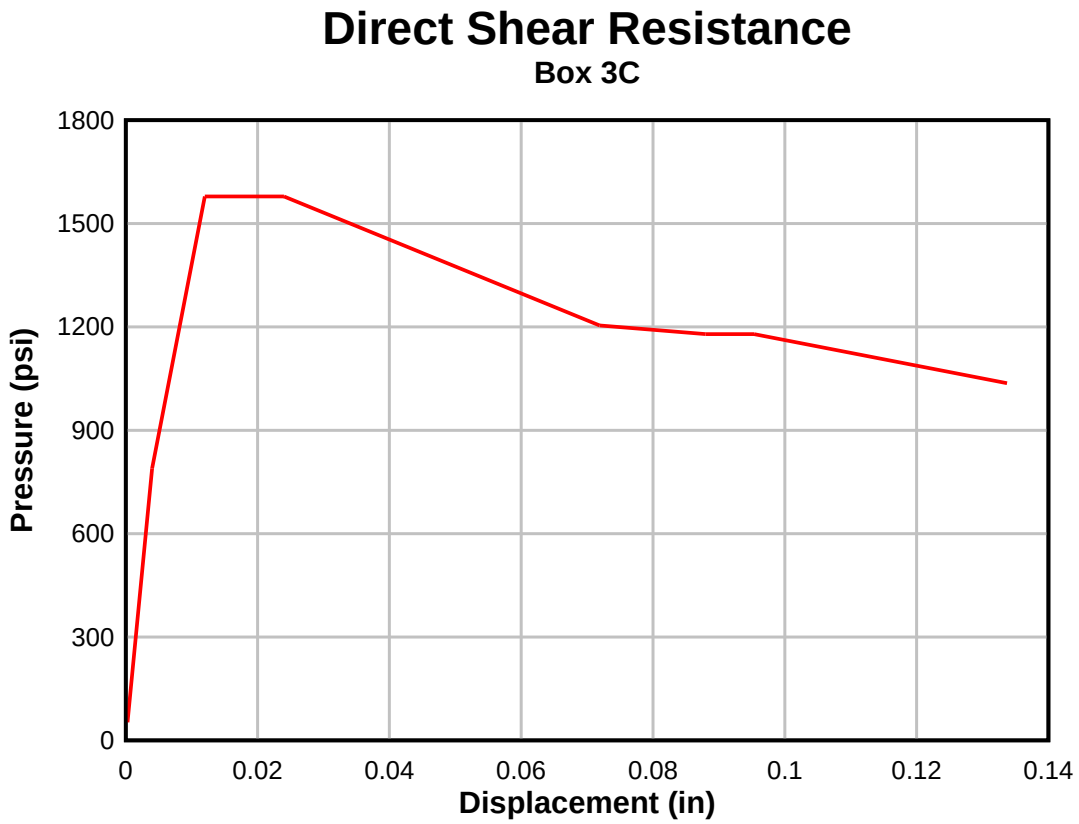

Figure 4-2. Direct shear resistance model for box 3C

4.2.2 Test Shots

All test shots shown here were located at the center of one of the longer sides of the boxes, at varying distances.

- Shot 3C1 was placed eight feet away from the wall center of box 3C. No structural damage was sustained.
- Shot 3C2 was located six feet from the wall center of box 3C. Moderate cracking was observed at the center of the wall section, with cracks radiating longitudinally along the wall. The damage is shown in Figure 4-3.
- Shot 3C3 was located four feet from the wall center opposite from the previous shots, so that an undamaged wall could be used. This portion of the wall, however, did not have a pressure gage. Since the distance was identical to shot 3D6, the load function from 3D6 is used in place of the unavailable date for 3C3 in this study. Problems presented by this substitution are explained in Section 4.2.4. This test resulted in a deflection in the wall of approximately 10.5 inches, with breaching assumed to be imminent. Researchers believed that this near failure response mode was flexure. The damage is shown in Figure 4-4.

- Shot 3D1 was located eight feet from the center of the long wall of box 3D. No damage was observed.

- Shot 3D2 was located six feet from the center of the long wall of box 3D. No damage was observed.

- Shot 3D6 was located four feet from the center of the long wall. It produced minor longitudinal cracks. The damage is shown in Figure 4-5.

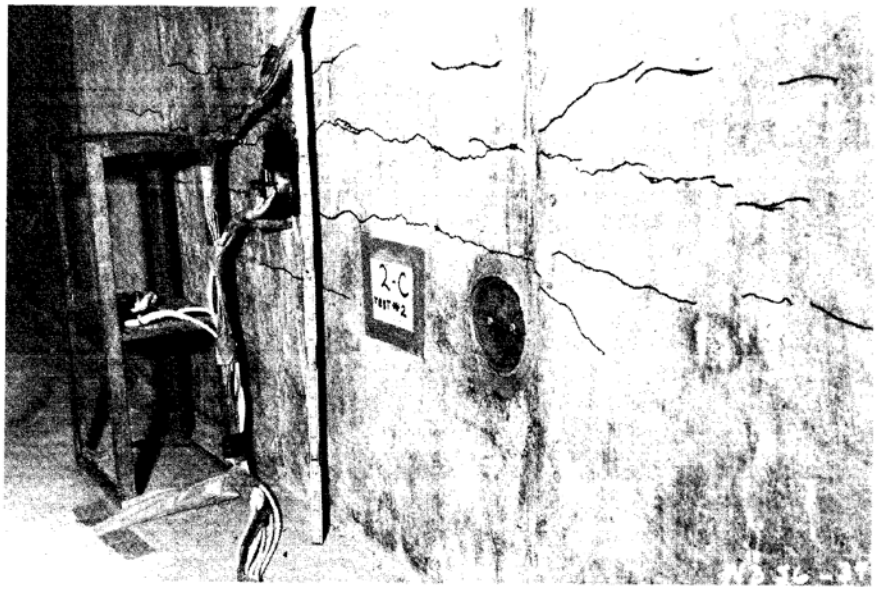

Figure 4-3. Damage after shot 3C2 (Kiger and Albritton 1980)

Figure 4-4. Near failure damage after shot 3C3 (Kiger and Albritton 1980)

Figure 4-5. Damage after shot 3D6 (Kiger and Albritton 1980)

The recorded pressure-time histories for the test shots are shown in Figure 4-6.

4.2.3 Calculated Deflection Histories

The loads shown above were digitized and input into DSAS, where they were applied to the proper structures. Figures 4-7 through 4-11 show the calculated deflection-time histories. A comparison with actual tests results is shown in the following section.

It should be noted that these are the pressures on the center of the wall, which are the greatest pressures felt anywhere with the configurations in this experiment. Therefore, using them as the loading function for the SDOF calculations overestimates the average pressure on the wall. Since no other pressure measurements on the wall are available, however, no more can be done without trying to assume an unverifiable factor to decrease the load.

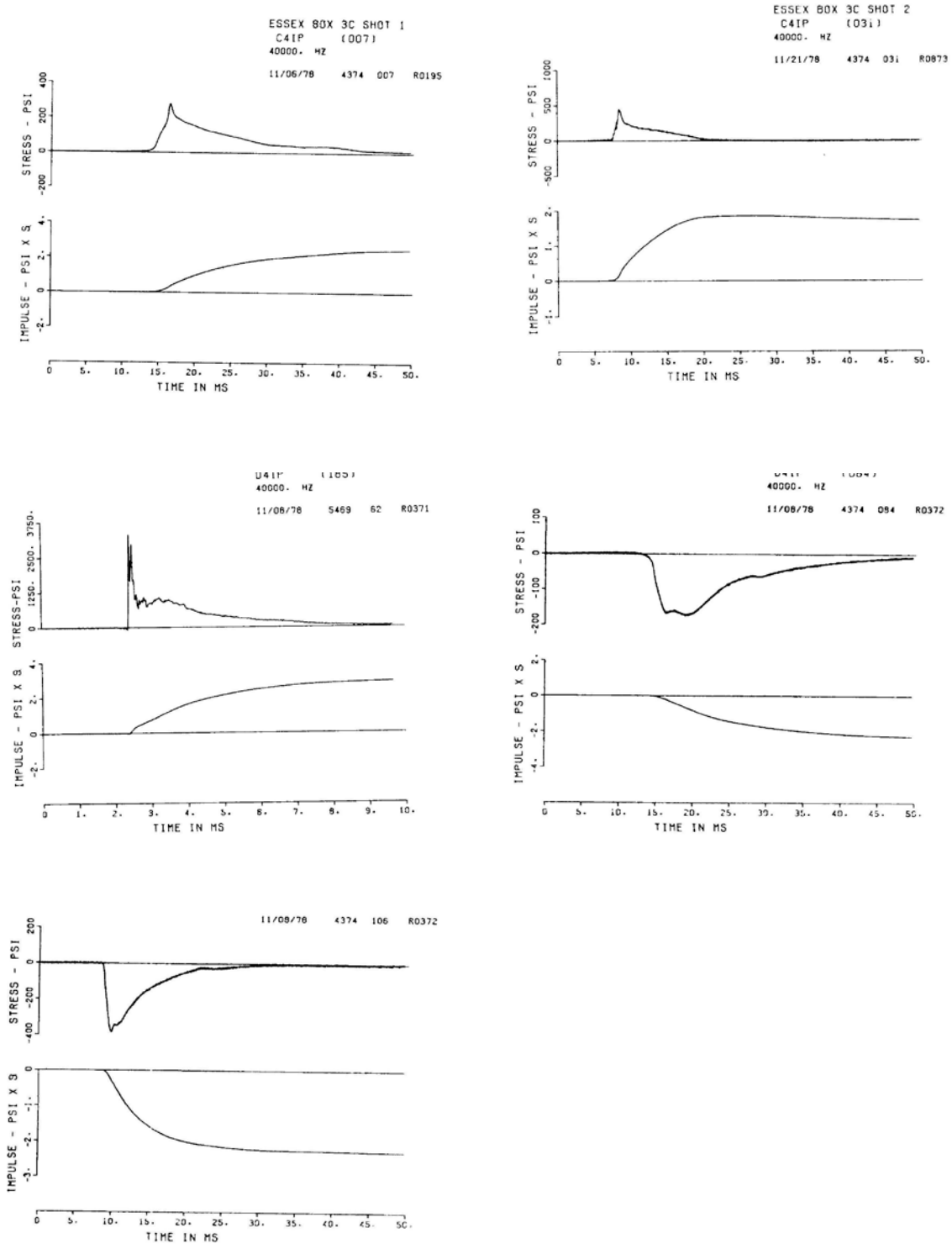

Figure 4-6. Experimentally measured pressure-time histories (Kiger and Albritton 1980)

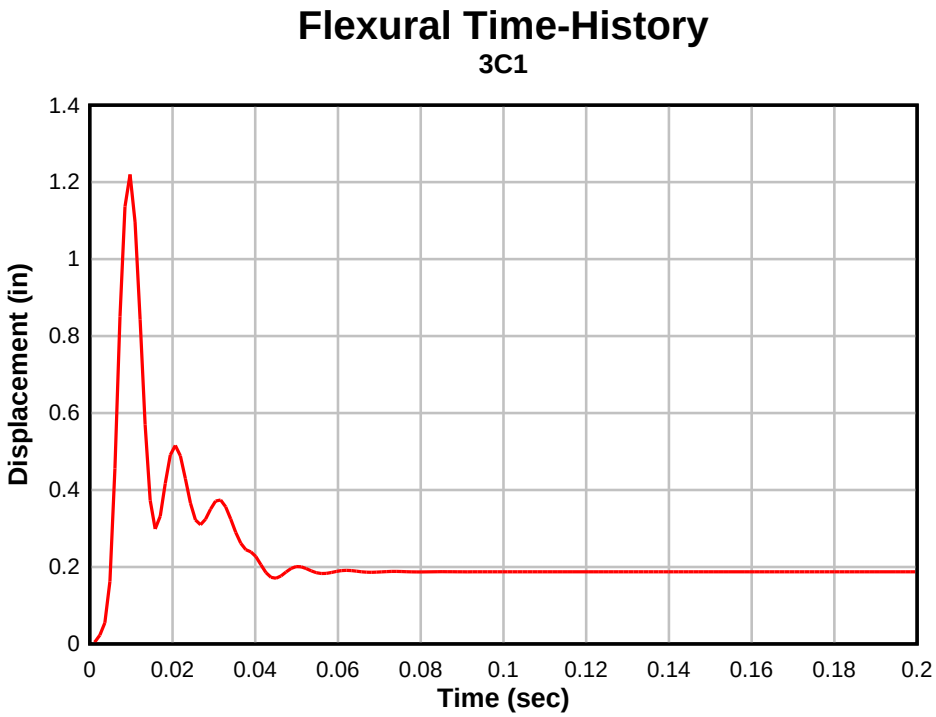

Figure 4-7. Calculated deflection-time history for test shot 3C1 from DSAS using digitized loads

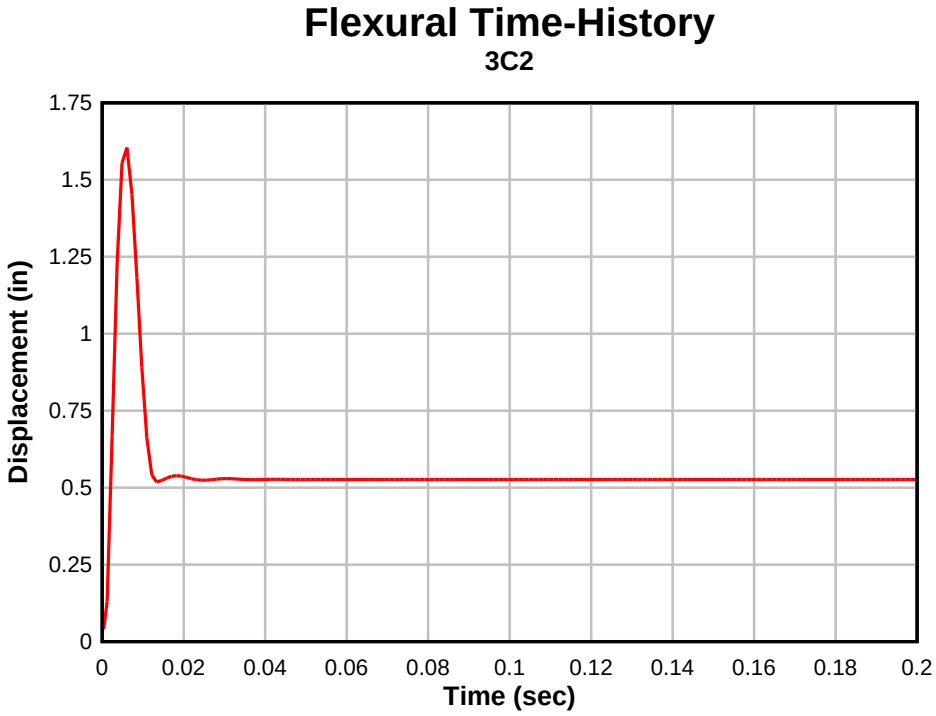

Figure 4-8. Calculated deflection-time history for test shot 3C2 from DSAS using digitized loads

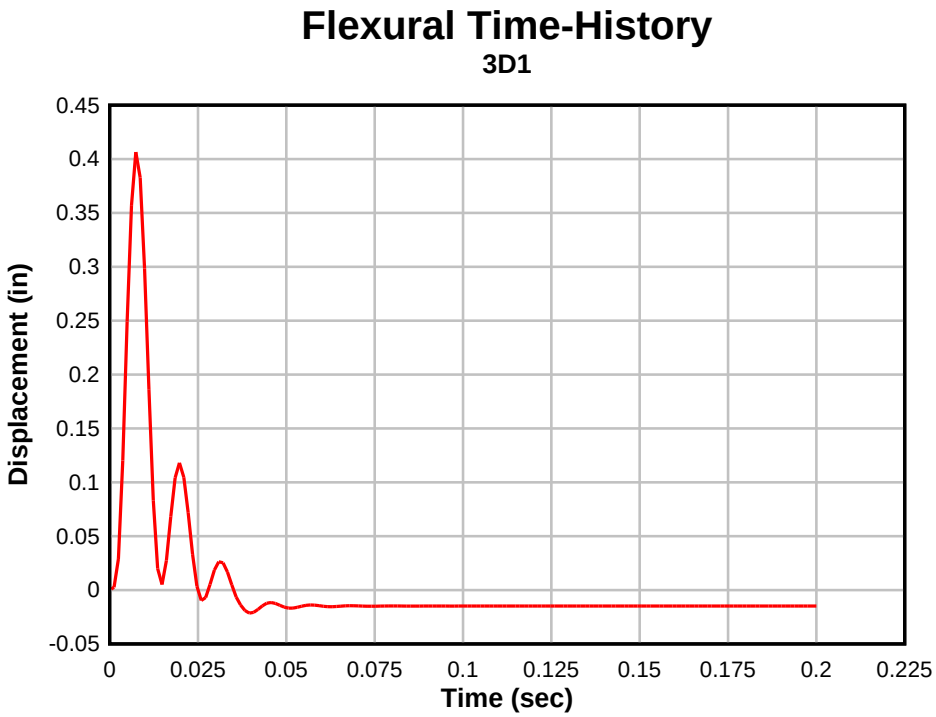

Figure 4-9. Calculated deflection-time history for test shot 3D1 from DSAS using digitized loads

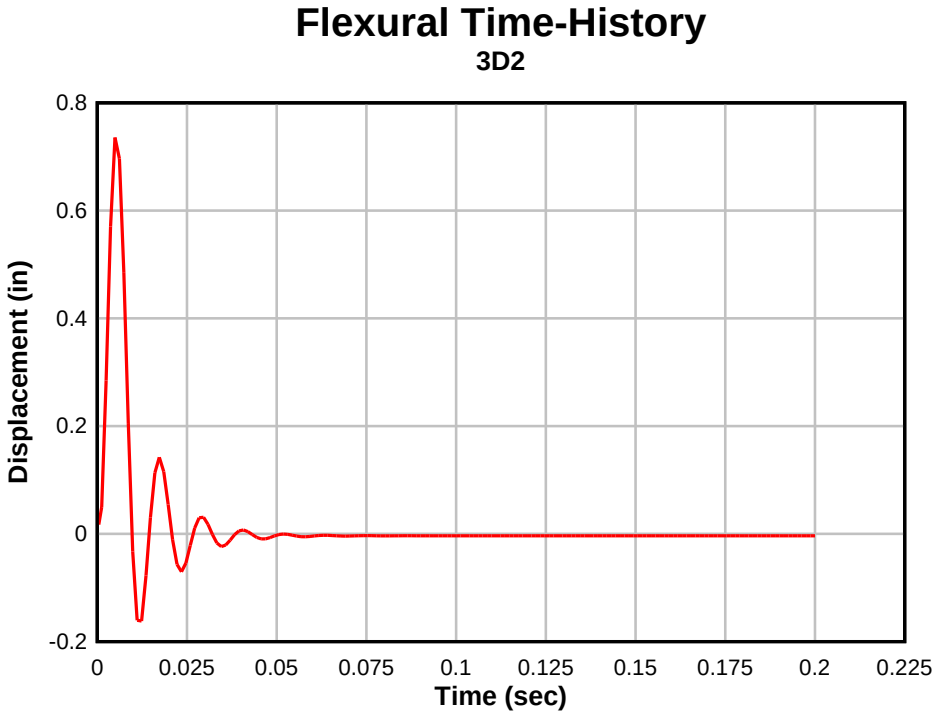

Figure 4-10. Calculated deflection-time history for test shot 3D2 from DSAS using digitized loads

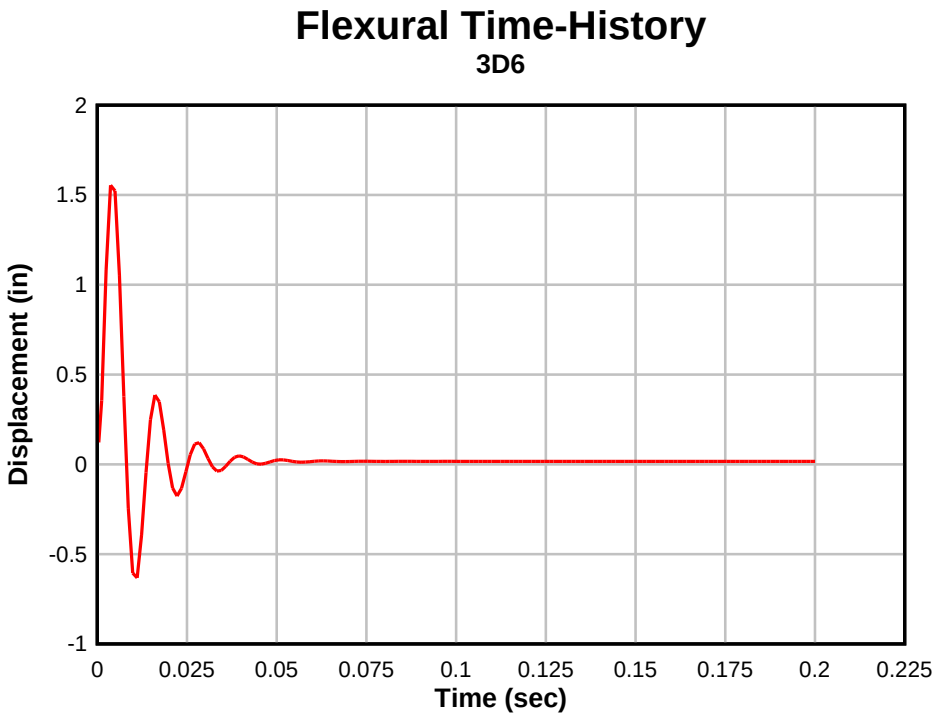

Figure 4-11. Calculated deflection-time history for test shot 3D6 from DSAS using digitized loads

4.2.4 Results Comparison

The maximum wall deflections from the output were used to calculate the walls' end rotations using the aforementioned 45° yield lines and the trigonometric equation:

$$\theta = \tan^{-1}\left(\frac{\Delta_{\max}}{0.5L}\right) \tag{4-1}$$

where L is the length of the shorter dimension of the box wall, Δ_{max} the maximum deflection, and θ the angle of rotation.

Using the following criteria for damage based on the end rotation of a slab found in UFC 3-340-02:

$0° \le \theta \le 2°$ Light damage
$0° \le \theta \le 6°$ Moderate damage
$6° \le \theta \le 12°$ Severe damage

expected damage could be determined. Calculation of expected damage was then compared against the recorded damage observations from the test report (Kiger and Albritton 1980) to validate the methods used in DSAS. This information is presented in Table 4-1.

Table 4-1. Validation results

Shot	Calculated Deflection (in)	L (in)	Calculated θ (degrees)	Calculated Damage Level	Observed Damage Level (from tests)	Calculated Final Deflection (in)
3C1	1.22	59.2	2.36	Moderate	No Damage	0.20
3C2	1.60	59.2	3.09	Moderate	Moderate Cracking	0.53
3C3*	9.02	59.2	17.95	Beyond Severe	Breaching imminent, permanent deflection of 10.5 inches	5.16
3D1	0.40	74.0	0.62	Light	No Damage	0.00
3D2	0.73	74.0	1.13	Light	No Damage	0.00
3D6	1.55	74.0	2.40	Moderate	Minor Cracking	0.02

*Shot 3C3 did not have a recorded pressure-time history. Since the charge used was located at a similar distance to the one used in 3D6, that pressure-time history was used for this comparison.

From this table, it can be seen that, in regards to the five tests with actual pressure-time histories, the program calculated a similar level of damage to that seen in the experiment. None of the boxes failed in direct shear according to the program and according to the experiment. Since no data for loading was available for a case with direct shear failure, the effectiveness of this portion of the program could not be determined.

Special consideration should be made for test 3C3. The deflection did not match what was observed; however, a true pressure-time history was not used. The loading used from shot 3D6 would have been similar to its actual load, but, as can be seen from the other tests, explosives at the same distances from the two boxes will not result in the same pressures. It should be noted that in preliminary tests using a less precise version the 3D6 loading, where the first spike, trough, and second spike were assumed as just one spike, the program showed the

box failing at a deflection of just over 10.5 inches. As it exists now, there was still more than a severe amount of damage.

4.3 Load Function Creation and Possible Improvement

As described in Chapter 2, semi-empirical equations exist for the calculation of the free-field pressures in soil. These equations were coded into DSAS. The results from DSAS matched well with those of an existing DOS version of the program ConWep. With validation of the first portion of the load function completed, additional modifications, discussed in Sections 3.4 and 3.5, were added.

Upon completion of the load-function-generating portion of DSAS, the results calculated using the experimental set-up were compared with the pressure-time histories measured during the Kiger and Albritton (1980) experiment. The values used in the calculations can be found at the end of the Appendix. Overlays of these results are shown in Figures 4-12 through 4-16.

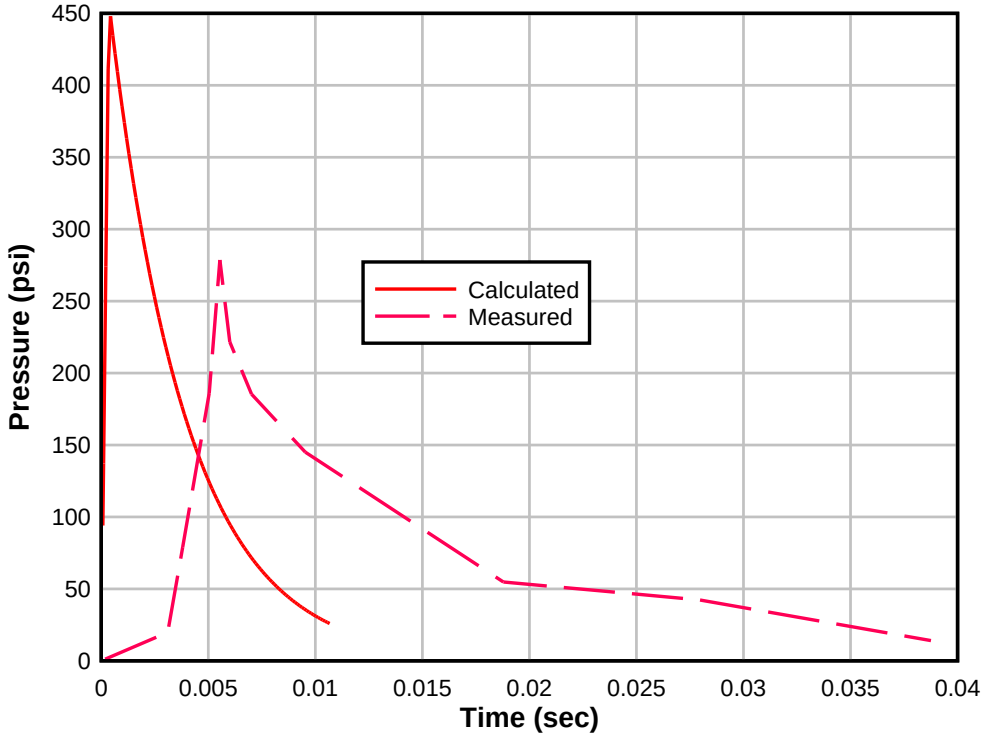

Figure 4-12. Overlay of original calculated load and digitized experimental load for test 3C1

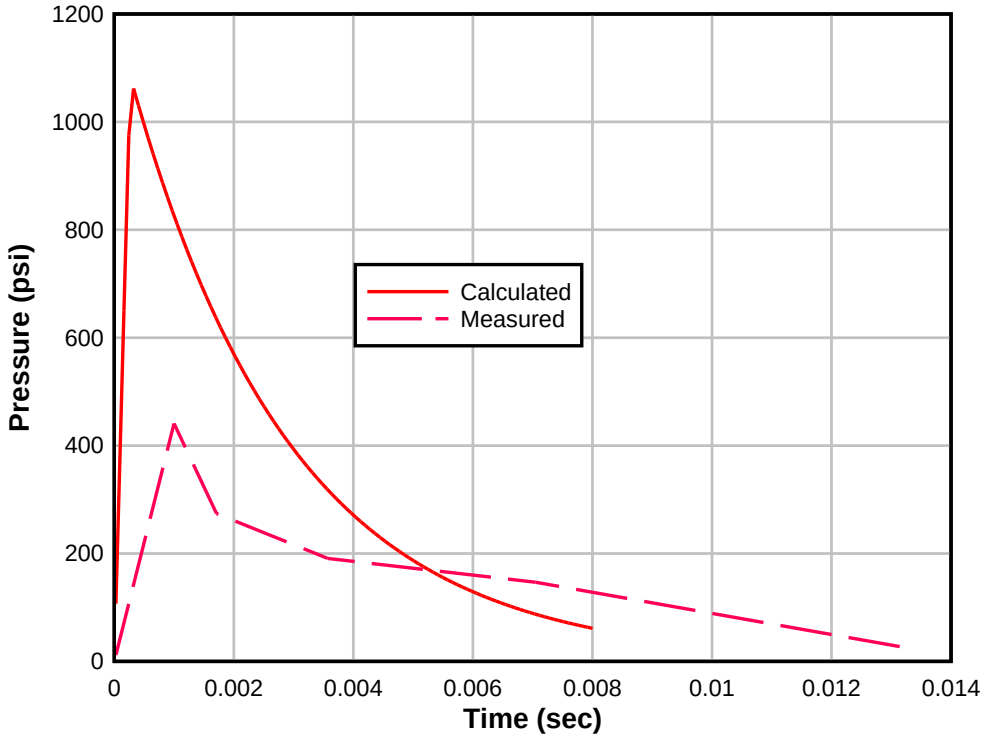

Figure 4-13. Overlay of original calculated load and digitized experimental load for test 3C2

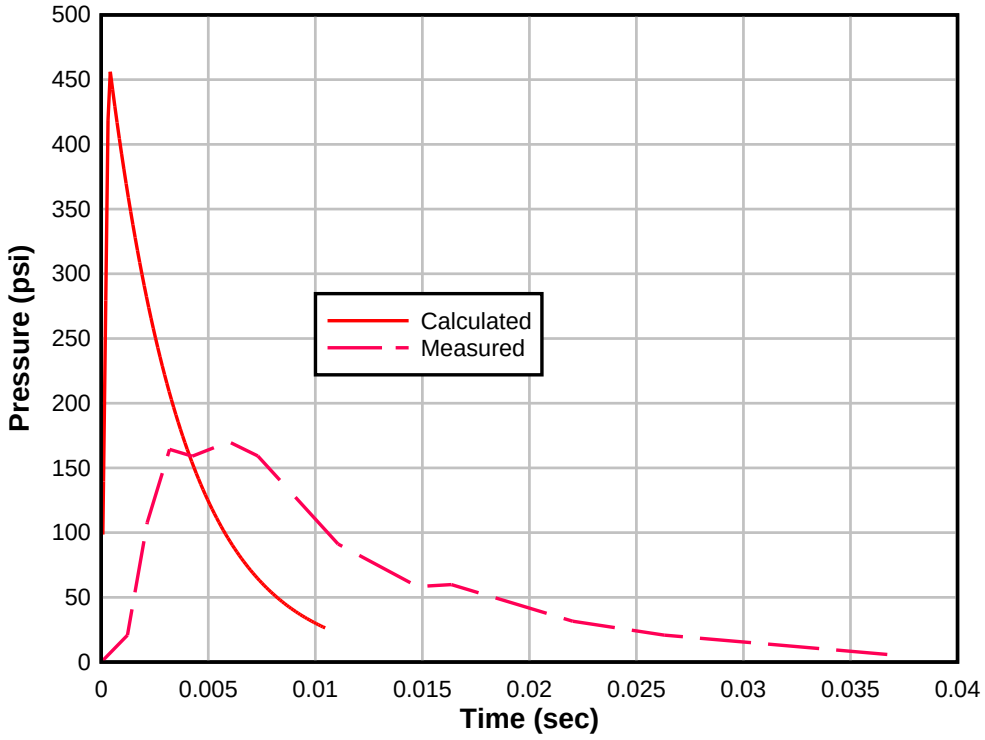

Figure 4-14. Overlay of original calculated load and digitized experimental load for test 3D1

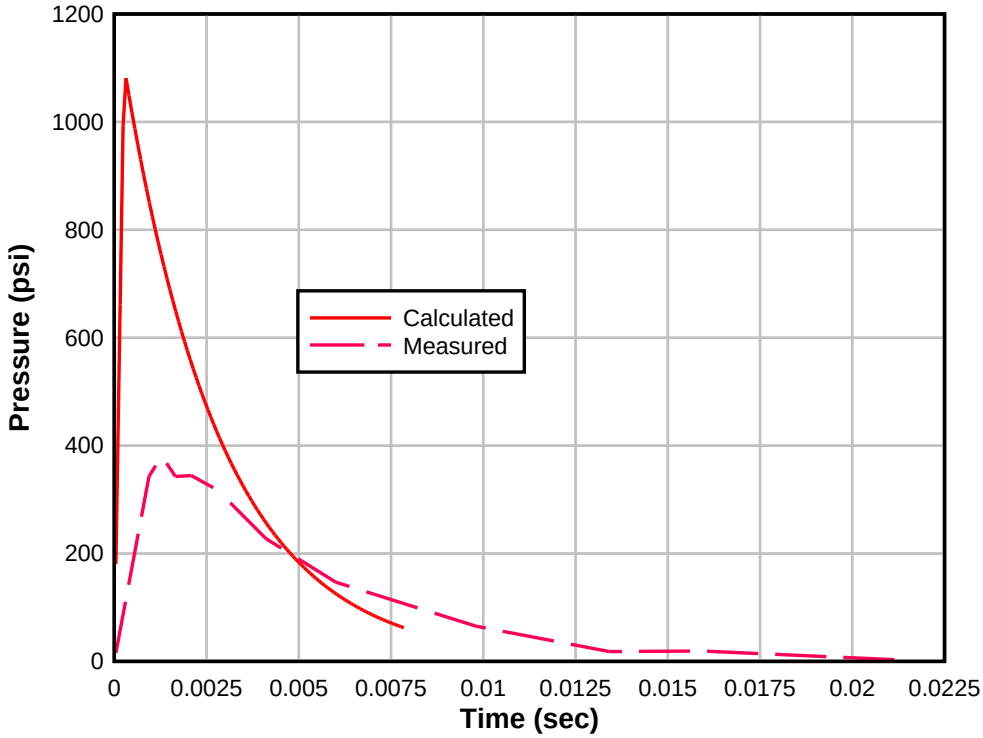

Figure 4-15. Overlay of original calculated load and digitized experimental load for test 3D2

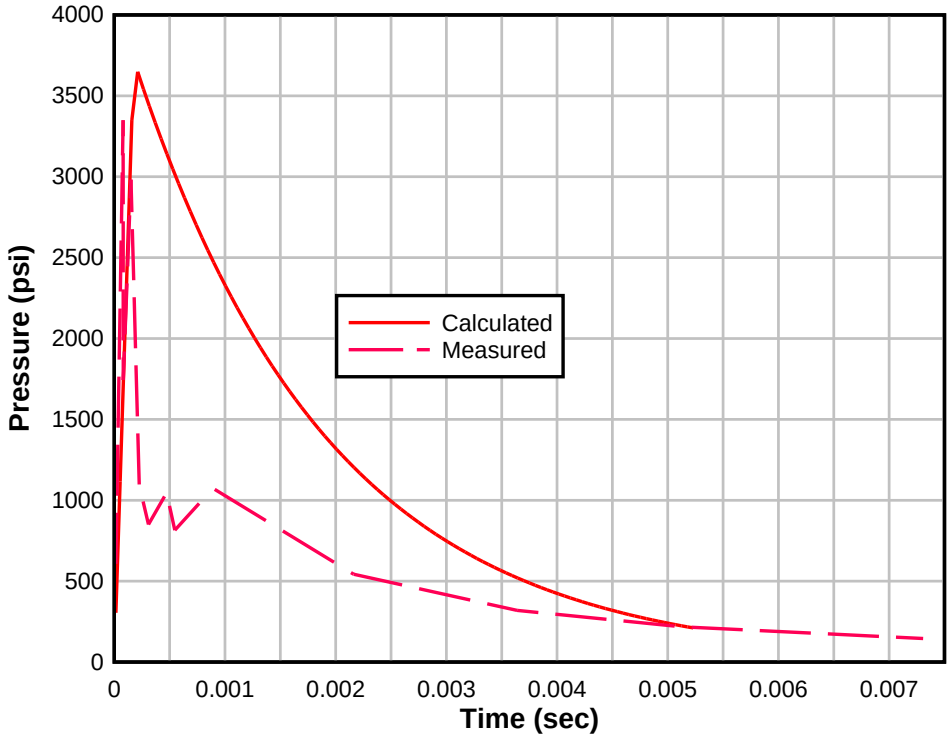

Figure 4-16. Overlay of original calculated load and digitized experimental load for test 3D6

In the pressure equations, the wave is assumed to be traveling at a speed equal to the soil's seismic velocity. However, the recorded pressure-time histories show that this is not the case. The arrival times shown on these graphs indicate a wave which has traveled at an average speed much lower than the seismic velocity, as little as three or four times slower. From the pressure equations, it can be seen that a wave traveling at a slower speed will exert less pressure. Since this pressure wave is not elastic and must use up energy by permanently crushing and moving soil, it would make sense that it would not travel at the same speed as waves used to measure seismic velocities (ESL-TR-87-57 1989).

The design manual recommends a rise time of approximately 10% of the arrival time. The test results indicate a much larger rise time. The rises shown are between 22% and 24% of the arrival time. This more than doubling of the rise time can have a large impact on the overall impulse.

To achieve better correlation between the analytical and experimental loads, the individual values used in the pressure calculations were modified for each case until the best match could be found. These best matched values are shown in Table 4-2.

Table 4-2. Best matched values

Test	c (ft/s)	n	Density (lbs/ft^3)	Rise Time (% of arrival time)	Decay Factor	Difference in Peak Pressure (psi) (Compared to Using Measured Pressures)	Difference in Max Deflection (in)	Difference in Permanent Deflection (in)
3C1	1400	3	112	45	e	21	0.15	0.104
3D1	750	2.75	112	20	e	14	0.06	0.006
3C2	600	3	112	15	e	49	0.068	0.007
3D2	1050	3.25	112	20	e	47	0.054	0.002
3D6	2100	3	112	10	30	90	0.14	0.013

While these value changes are a great improvement over the existing method, they are still somewhat inaccurate. Although the change in rise time can be easily adopted into the methodology, a way to calculate these average wave speeds using only the soil and charge data has not been determined. An example comparison of one of these best fit values and the recorded data is shown in Figure 4-17.

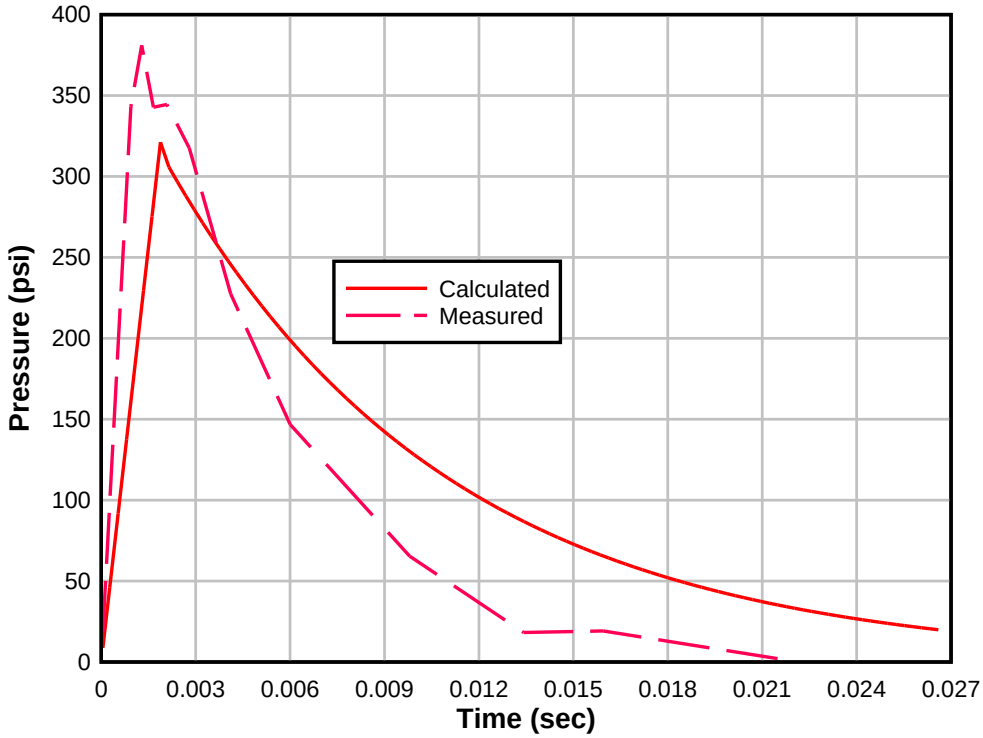

Figure 4-17. Overlay of best fit calculation and digitized experimental load from test 3D2

Because the only pressure data recorded during the experiments occurred at the center point of the wall, the only valid comparison is one whose pressure is calculated by DSAS only at the center point of the wall. The calculated average loads on the wall's surface could not be validated against any real-world data, since none is available. Figure 4-18 shows the difference between the calculated average load on the wall's face and the central load. These loading functions come from the original calculated load from shot 3C1.

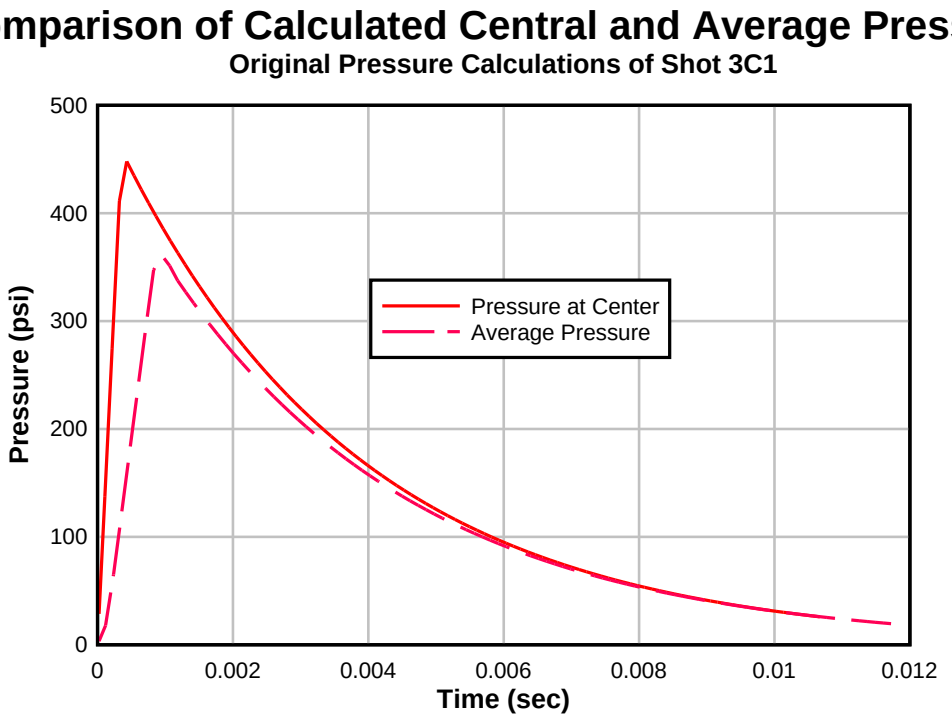

Figure 4-18. Comparison of calculated pressure at the wall center and calculated average pressure

4.4 Summary

In this chapter, the methods proposed in Chapter 3 were compared with experimental results. The results obtained from DSAS were in good agreement with the behavior observed in the experiments when the pressure-time histories obtained in the actual experiments were used as input for DSAS. However, when the loading was generated using the approach described in this chapter, the correlation between the pressures generated by DSAS and the pressures that were measured in the experiments was poor. Modifications were suggested, which helped create a closer match to the test data. Although an improvement, these methods are still not entirely accurate, and a method to calculate these new functions using only soil and charge data was unable to be created.

CHAPTER 5
CONCLUSION AND RECOMMENDATIONS

5.1 Summary

A numerical method for analyzing the response of an RC box-type structure subjected to loading from a buried high energy explosive was developed in this study. This method uses a pair of SDOF models to model the flexure and direct shear modes of response on a selected box wall. An attempt was made to calculate the forcing function created by a buried explosive. A method using existing, semi-empirical equations did not compare well with experimental results. Changes to these existing equations were investigated for improvements. While improvements could be made, a pattern that could be used to modify the equations for every case could not be found.

Background information on RC boxes and underground blast loading was presented in Chapter 2. The assumptions used in adapting a wall into a SDOF system were discussed. Possible failure modes, namely flexure and direct shear, were presented. The methods for calculating free-field soil pressures using elastic wave reflections and transmissions were described.

The proposed methodology for creating the two SDOF systems was discussed in Chapter 3. Methods for creating flexural and direct shear resistance functions were presented. Modifications to the free-field soil equations and wave behavior in order to generate a single loading function on the wall were also discussed.

Experimental data was used to validate the direct shear and flexural response models, once their methods had been coded into the computer program DSAS. Validation for flexure was found, but no experimental data containing direct shear behavior could be found to validate the direct shear methods. An attempt was made to validate the methodology used in creating a

load function, but a good comparison to experimental data was not found. Further improvements were made to the load function calculations for each individual case, but a pattern that could be used to develop an improved method for every case could not be found.

5.2 Conclusions

The following conclusions could be made from this study:

- Provided the actual load-time history, the SDOF analysis engine in DSAS can produce accurate results.
- The existing methodology for calculating pressure in soils caused by a below-ground detonation is not accurate. Two reasons for this can be verified from experimental data: on average, the blast wave appears to be traveling at a rate much slower than the soil's seismic velocity, and rise time is greater than 10%. Furthermore, the change in soil density due to compaction by the pressure wave and the nonlinear propagation of a pressure wave also need to be considered for a more accurate analysis.

5.3 Recommendations for Further Study

Based on the knowledge gained from the work completed, the following recommendations for further study can be made:

- This study was focused on the central part of the walls of a buried box; possible research into the responses of corners where the walls or the walls and roof meet, is worth pursuing.
- More research into properly calculating the loading functions caused by a buried explosive should be performed, including a look into how changing any of the different variables will change the pressure-time history. Specifically, research into calculating the wave's actual propagation speed is important. Also, a look into how to calculate a more appropriate rise time would be helpful.
- The possibility of soil arching affecting the load should be studied further. As existing methods to simplify soil arching effects are based on the assumption of a uniformly distributed load, they cannot be used in their current form.
- Since available experimental data does not include the average load on the wall, validation of the methodology used in creating an average loading function for SDOF systems could not be completed. When this data is obtained, validation should be performed.
- Additional experiments need to be performed with real buried structures, especially experiments where direct shear failure is likely to occur, and experiments using a variety

of soil backfills, with extensive soil data collected both before and after the explosion, so that these methods for calculating loading and response functions can be further verified. These experiments should also include pressure gages located throughout the wall, not just on the wall's center, as well as gages to measure the wall's deflection.

APPENDIX
KIGER AND ALBRITTON (1980) TESTS

The experimental tests used in the validation work are further explained in this section. This includes detailed information on the box compositions, the soil, the test shots and data recorded in each, and the data used for the test calculations. The reason these last values are included is that, at times, a large range of possible values is given in the report. At other times, some information is not included at all. Therefore, the values used in the actual input files need to be listed.

Box Compositions

Two boxes were used in these experiments, known as Structure 3C and 3D. The dimensions and layouts of the boxes were different, but the properties of the materials used were the same.

The compressive strength of the concrete in Structure 3C was 6,595 psi. In 3D it was 6,613 psi. The No. 4 bars used had an average yield stress of 76,000 psi and an ultimate stress of 124,000 psi. For the No. 6 bars, the yield stress was 71,000 psi and the ultimate stress was 128,000 psi. The typical stress-strain curves are shown in Figures A-1 and A-2.

For both boxes, the interior dimensions were 4 feet high by 4 feet wide by 16 feet long. Structure 3C had a wall thickness of 5.6 inches. This includes the thickness of the roof and floor. The wall thickness in structure 3D was 13 inches.

The transverse reinforcement of Structure 3C consisted of No. 4 bars spaced at 4 inches on center in both faces and all four sides. Longitudinal reinforcement consisted of No. 3 bars spaced at 4 inches on center in both faces and all four sides. Shear reinforcement consisted of No. 3 bar shear stirrups spaced at 4 inches on center.

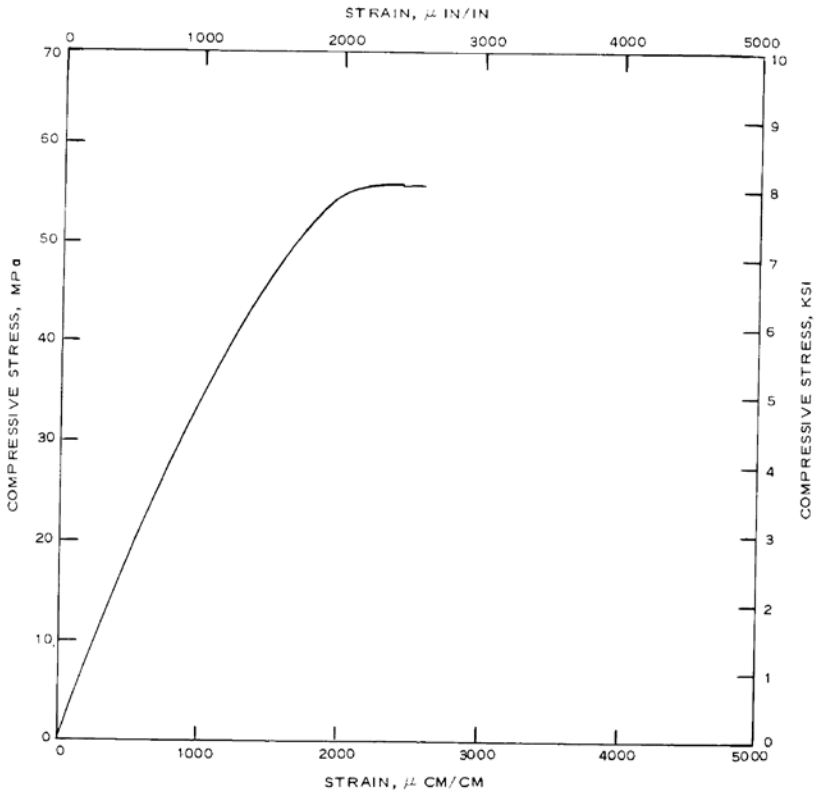

Figure A-1. Typical concrete stress-strain curve (Kiger and Albritton 1980)

The transverse reinforcement of Structure 3D consisted of No. 6 bars spaced at 4 inches on center in both faces and all four sides. Longitudinal reinforcement consisted of No. 3 bars spaced at 4 inches on center in both faces and all four sides. Shear reinforcement consisted of No. 3 bar shear stirrups spaced at 4 inches on center.

Sketches of these layouts can be seen in Figure A-3.

Soils

At the test site, there were two major regions of soils, although a silty sand was encountered at 10 feet. No thickness or seismic velocity is given for this silty sand. The top layer of soil is a clayey, silty sand. It has a wave velocity of 1345 to 1360 ft/s. This layer exists for a depth of 3 feet. The second layer is a red or tan sandy clay. It has a wave velocity of 2360

to 2590 ft/s. This soil layer exists from a depth of 3 feet to 26 feet. However, on the test day, the water table was located at a depth of 24 feet.

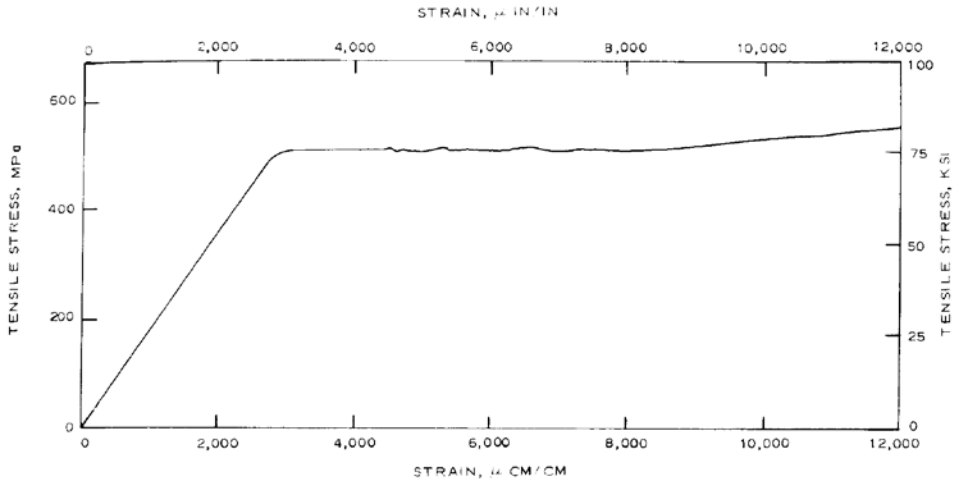

a. No. 4 reinforcing bar.

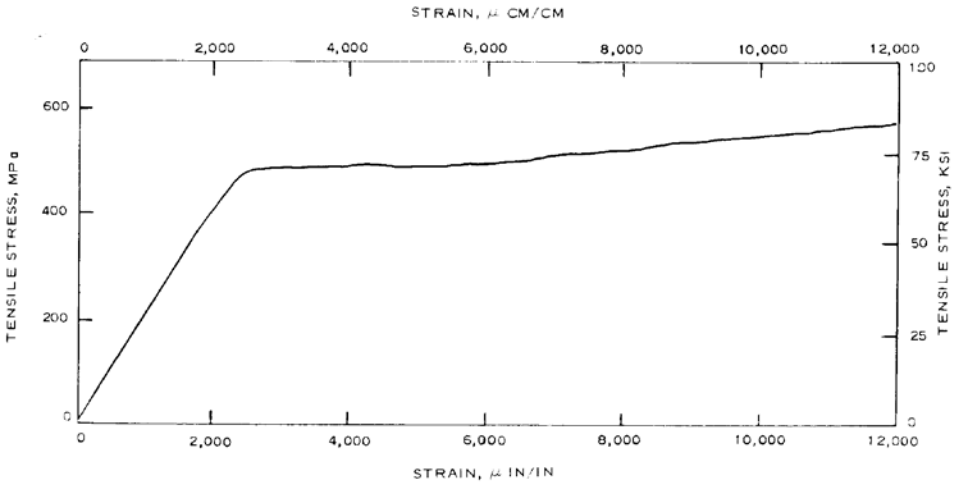

b. No. 6 reinforcing bar.

Figure A-2. Steel stress-strain curve (Kiger and Albritton 1980)

Test Shots and Data Recording

Although many test shots were performed on the structures, only six of these shots were used in this study. There were numerous gages set up throughout the boxes, but only one pressure gage per box. These pressure gages were located at the center of one of the long walls

of each box. Also located at the center of the long walls, but on the interior side, was an accelerometer. The researchers tried to integrate the accelerometer data to calculate the wall deflections, but the results do not appear to be accurate.

Only five test shots were placed adjacent to the wall with the pressure sensor. These were shots 1 and 2 on Structure 3C (3C1 and 3C2) and shots 1, 2, and 6 on Structure 3D (3D1, 3D2, and 3D6). Shot 3 on Structure 3C (3C3) was also located on a long box wall, but not on the one with the pressure sensor. The researchers had decided that the second shot had done too much damage to the wall and the use of a fresh wall was necessary to obtain good data. Diagrams of instrumentation and shot locations can be seen in Figures A-4 and A-5.

Values Used in Computer Calculations

Table A-1 lists the input values used in the original calculations with the test date. These values were used for both boxes unless otherwise noted.

Table A-1. List of values used in computer calculations

Item	Value	Unit
Interior Length X	203.2	in
Interior Length Y	59.2	in
Interior Length Z	59.2	in
Burial Depth	24	in
Wall, Floor, Roof Thicknesses, Box 3C	5.6	in
Wall, Floor, Roof Thicknesses, Box 3D	13	in
Concrete f'c	7500	psi
Steel Yield	75000	psi
Steel Ultimate	90000	psi
Steel Strain Hardening	0.00275	in/in
Steel Ultimate Strain	0.12	in/in
Steel Failure Strain	0.15	in/in
Wall Rebar Z, Box 3C	#4	bar #
Wall Rebar Z, Box 3D	#6	bar #
Wall Rebar X	#3	bar #
Rebar Spacing (all)	4	in
Outer Rebar Depth	0.8	in
Inner Rebar Depth	4.8	in

Table A-1 Continued.

Item	Value	Unit
Wave Reflection from Surface	yes	
First Soil Layer Thickness	36	in
First Soil Layer Unit Weight	110	lb/ft^3
First Soil Layer Seismic Velocity	1350	ft/s
First Soil Layer Attenuation Coefficient	3	
First Soil Layer Friction Angle	30	degrees
Second Soil Layer Thickness	252	in
Second Soil Layer Unit Weight	112	lb/ft^3
Second Soil Layer Seismic Velocity	2450	ft/s
Second Soil Layer Attenuation Coefficient	3	
Second Soil Layer Friction Angle	30	degrees
Third Soil Layer Thickness	300	in
Third Soil Layer Unit Weight	125	lb/ft^3
Third Soil Layer Seismic Velocity	2450	ft/s
Third Soil Layer Attenuation Coefficient	3	
Third Soil Layer Friction Angle	30	degrees
Flexural Damping	20	%
Direct Shear	5	%

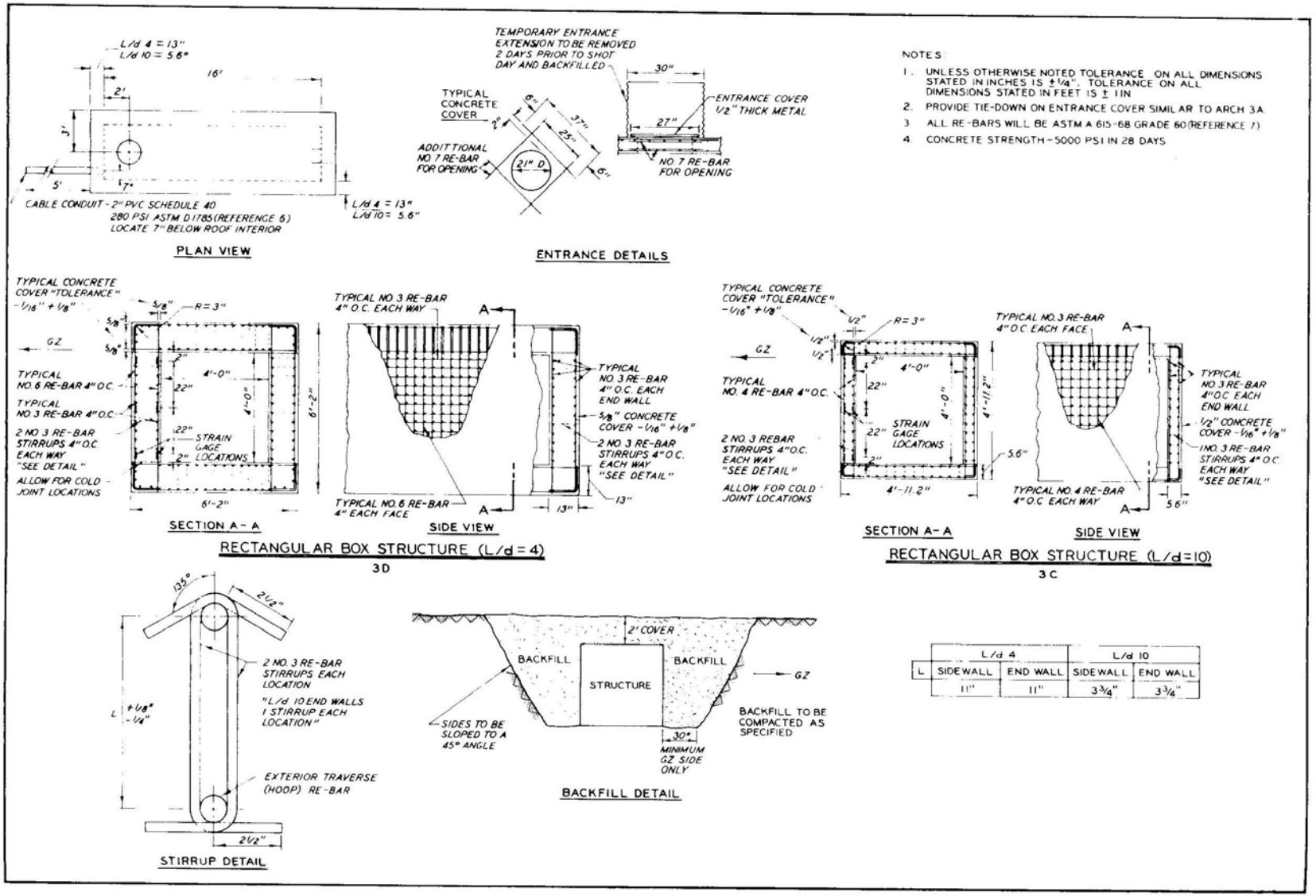

Figure A-3. Box layouts (Kiger and Albritton 1980)

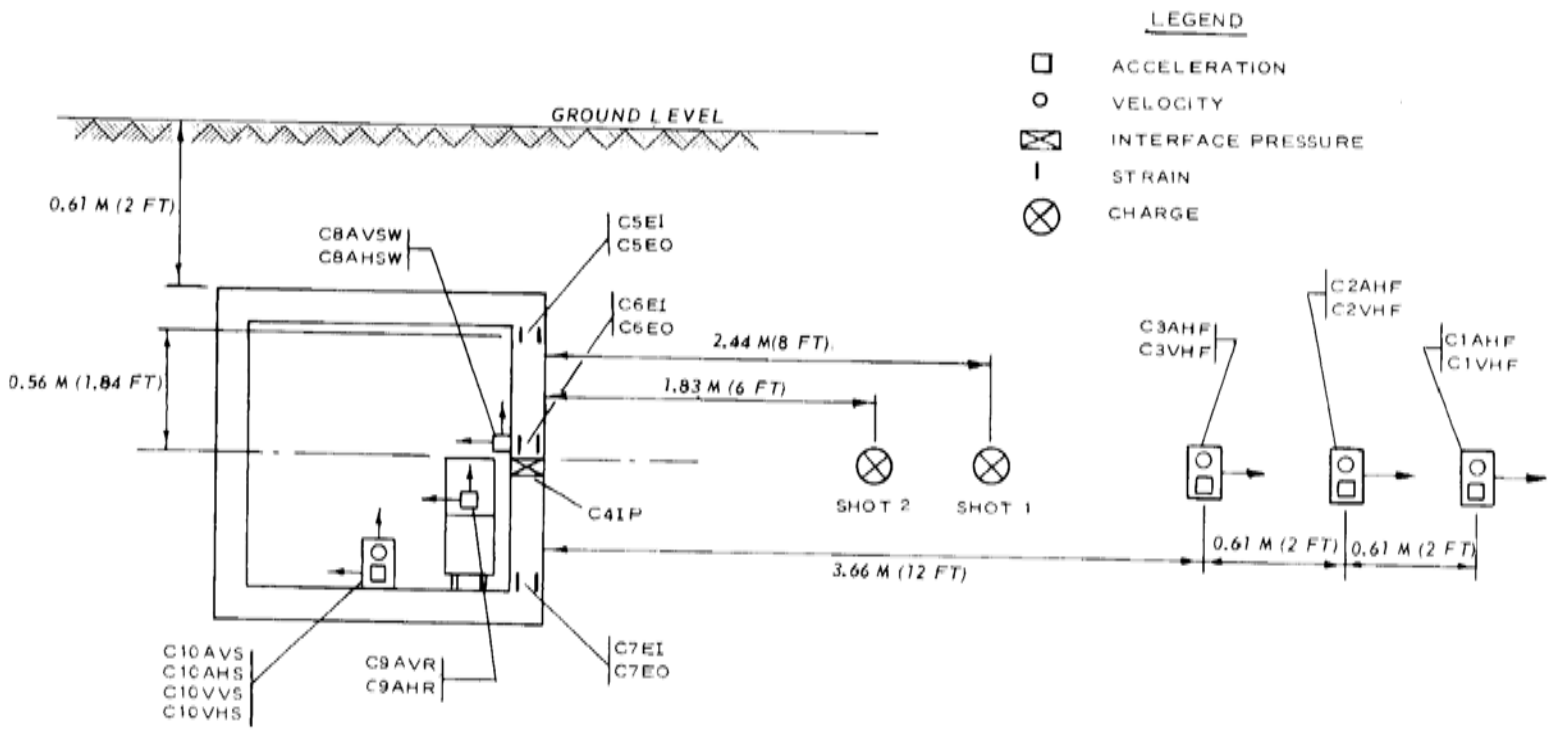

Figure A-4. Shot and instrumentation layouts, box 3C (Kiger and Albritton 1980)

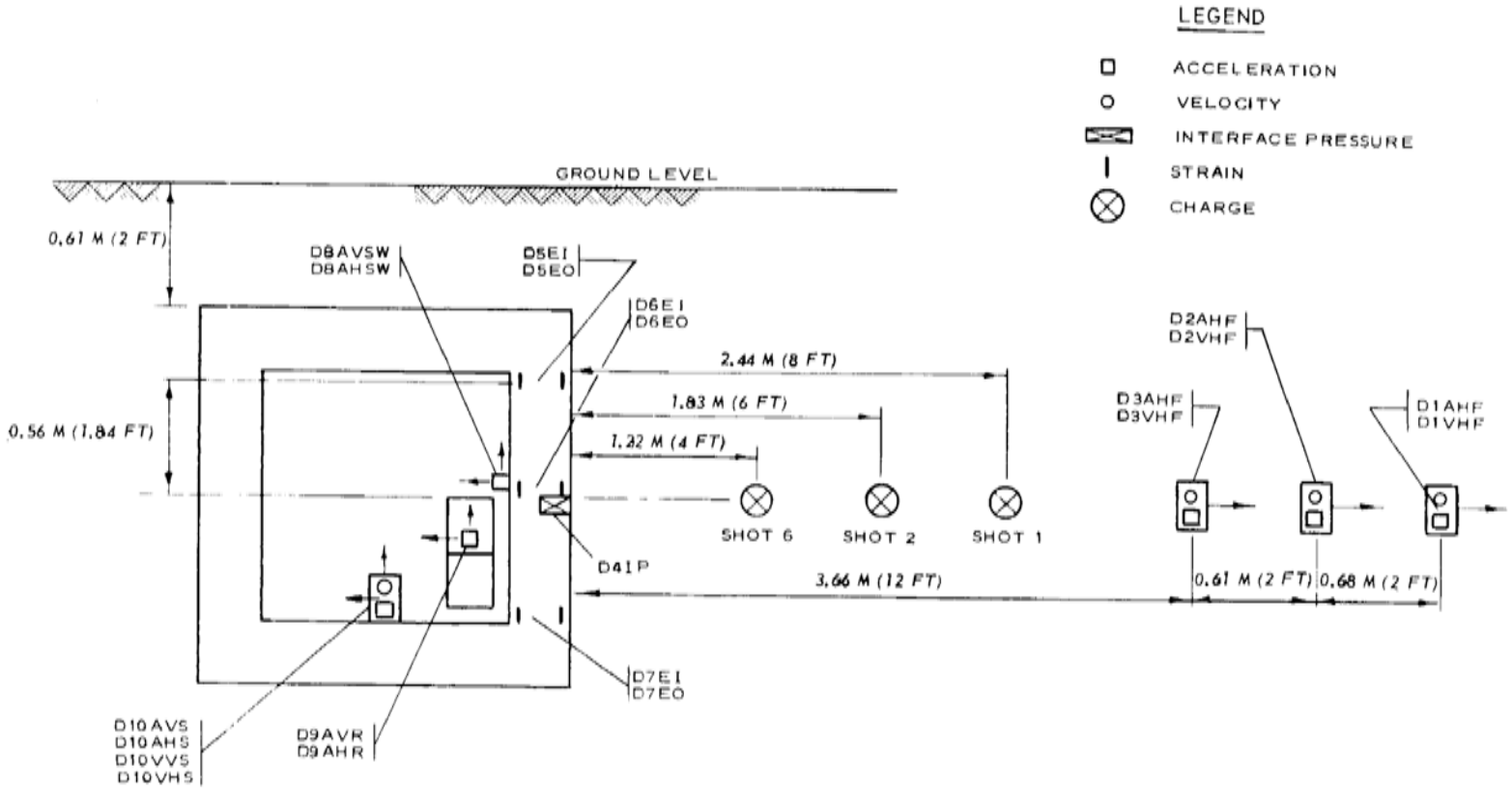

Figure A-5. Shot and instrumentation layouts, box 3D (Kiger and Albritton 1980)

LIST OF REFERENCES

Astarlioglu, S., and Krauthammer, T. “Dynamic Structural Analysis Suite (DSAS).” Center for Infrastructure Protection and Physical Security, University of Florida, 2009.

Biggs, John M. Introduction to Structural Dynamics. New York: McGraw-Hill, 1964.

"Design of Structures to Resist Nuclear Weapon " 1985, ASCE Manuals and Reports on Engineering Practice No. 42, ASCE

Hyde, D., ConWep- Application of TM5-855-1. Structural Mechanics Division, Structures Laboratory, USAE Waterways Experiment Station, Vicksburg, Mississippi, 1992.

Kiger, S. A., and Albritton, G.E., “Response of Buried Hardened Box Structures to the Effects of Localized Explosions”, U.S. Army Engineer Waterways Experiments Station, Technical Report SL-80-1, March 1980.

Krauthammer, T. Modern Protective Structures. CRC Press, 2008.

Krauthammer, T., et al., 1986 “Modified SDOF Analysis of R. C. Box-Type Structures” *Journal of Structural Engineering*, Vol. 112, No. 4, pgs 726-744

Krauthammer, T. and W.J. Hall, 1982. “Modified Analysis of Reinforced Concrete Beams” *Proceedings of the ASCE- Journal of the Structural Division*, Vol. 108, No. 2, pgs 457-474

Krauthammer, T. and Mehul Parikh, 2005 “Structural Response Under Localized Dynamic Loads” *Proceedings of Second Symposium on the Interaction of Non-Nuclear Munitions with Structures*, pgs. 52-55

MacGregor, J.G. and J.K. Wight Reinforced Concrete: Mechanics and Design. Upper Saddle River, N.J.: Prentice Hall 2005.

Newmark, N., et al., 1962 “A Method of Computation for Structural Dynamics” *American Society of Civil Engineers Transactions*, Vol. 127, Part 1, pgs 601-630

Park, Robert and Thomas Paulay. Reinforced Concrete Structures. New York: John Wiley & Sons, Inc., 1975.

Park, Robert and William L. Gamble. Reinforced Concrete Slabs. New York: John Wiley & Sons, Inc., 2000.

Parikh, Mehul and T. Krauthammer, 1987 “Behavior of Buried Reinforced Concrete Boxes Under the Effects of Localized HE Detonations” Structural Engineering Report ST-87-02, University of Minnesota, Department of Civil and Mineral Engineering Institute of Technology

“Protective Construction Design Manual” 1989, ESL-TR-87-57, U.S. Air Force Engineering and Services Center, Engineering and Services Laboratory, Tyndall Air Force Base, Florida.

"Structures to Resist the Effects of Accidental Explosions" 2008, UFC 3-340-02

Tedesco, Joseph W. et al. Structural Dynamics: Theory and Applications. California: Addison-Wesley, 1999.

Terzaghi, K. and R.B. Peck. Soil Mechanics in Engineering. New York: Wiley, 1949.

BIOGRAPHICAL SKETCH

Nick Henriquez was born in Tampa, Florida in 1984. He stayed in Tampa, where he graduated from Jesuit High School in 2003. Nick enrolled at the University of Florida in 2003, completing a Bachelor of Science degree in civil engineering in 2007. During his time as an undergraduate, he became a member of Sigma Nu fraternity. In 2008, at the University of Florida, he began the pursuit of a Master of Science degree in civil engineering with an emphasis in protective structures. While seeking this degree, Nick has worked as a research assistant at UF's Center for Infrastructure Protection and Physical Security (CIPPS).